STUDY OF MECHANICAL PERFORMANCE OF STENT IMPLANTS USING THEORETICAL AND NUMERICAL APPROACH

Hua Yang

Thesis Prepared for the Degree of

MASTER OF SCIENCE

UNIVERSITY OF NORTH TEXAS

August 2015

APPROVED:

Aleksandra Fortier, Major Professor
Kyle Horne, Committee Member
Samir Aouadi, Committee Member
Yong Tao, Chair of the Department of Mechanical and Energy Engineering
Costas Tsatsoulis, Dean of the College of Engineering and Interim Dean of Toulouse Graduate School

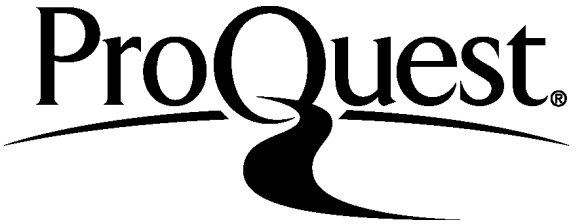

Yang, Hua. *Study of Mechanical Performance of Stent Implants Using Theoretical and Numerical Approach*. Master of Science (Mechanical Engineering), August 2015, 82 pp, 8 tables, 50 figures, references, 97 titles.

Coronary heart disease kills more than 350,000 persons/year and it costs $108.9 billion for the United States each year. In spite of significant advancements in clinical care and education for public, cardiovascular diseases (CVDs) are the leading cause of death and disability in the nation. Cardiovascular disease involves mainly heart or blood vessels (arteries, veins and capillaries) or both, and then mainly occurs in selected regions and affects heart, brain, kidney and peripheral arteries. As a surgical intervention, stent implantation is deployed to cure or ameliorate the disease. However, the high failure rate of stents used in patients with peripheral artery diseases has lead researchers to give special attention towards analyzing stent structure and characteristics.

In this research, the mechanical properties of a stent based on the rhombus structure were analyzed and verified by means of analytical and numerical approaches. Theoretical models based on the beam theory were developed and numerical models were used to analyze the response of these structures under various and complex loading conditions. Moreover, the analysis of the stent inflation involves large deformations and large strains. Nonlinear material properties also need to be considered to accurately capture the deformation process. The maximum stress values were found to occur in localized regions of the stent. These regions were generally found along the inner radii of each of the connected links connecting each of the longitudinal struts. Stress values throughout the whole stent were typically much lower. The peak engineering stress values were found to be less than the material ultimate strength (limit stress 515Mpa), indicating a safe stent design throughout expansion range. Lastly, the rheological behavior of blood can be quantified by non-Newtonian viscosity. Carreau model is introduced and simulates the situation in the artery,

ACKNOWLEDGEMENT

There are no proper words to express my gratitude to Dr. Aleksandra Fortier and Dr. Kyle Horne for providing me all of the support, advice, and opportunities though these two years of research, Dr. Xu Nie generously provide one semester RA support for me. Thanks to all of them for encouraging me to have my own opinion about this research. I'd also need to thank Dr. Samir Auadi for reviewing my thesis, Dr. Ju and Julian Quintero for providing me suggestion and help on this research.

Thanks to UT Southwestern Dr. Banerjee and his medical team provide the IVUS data.

Thanks to my friends and colleagues for helping me when I am in trouble.

Last but not least, I really appreciate what my family members and my parents had done for me. Without their support and encouragement, I don't have such courage to continue my study aboard.

TABLE OF CONTENTS

Page

LIST OF TABLES

Page

LIST OF FIGURES

Page

CHAPTER 1

INTRODUCTION

1.1 Background

Heart diseases are a major cause of death with about 600,000 deaths per year. Among them, a coronary heart disease alone kills more than 350,000/year and it costs $108.9 billion for the United States each year which includes the cost of health care services, medications and lost productivity [1]. These costs are mainly attributed to the medications and treatments needed for patients. In spite of significant advancements in clinical care and education for public, cardiovascular diseases (CVD) are leading cause of death and disability to the nation. Cardiovascular diseases (CVDs) include peripheral artery disease (PAD), high blood pressure (HBP), coronary heart disease (CHD), heart failure (HF) and stroke. Nearly 2400 Americans die of CVDs each day [2] (an average of 1 death every 37 seconds). A cardiovascular disease involves mainly heart or blood vessels (arteries, veins and capillaries) or both. The diseases occur in selected regions and affects heart, brain, kidney and peripheral arteries. The symptoms of CVD will depend upon the location of the disease. Most of the CVDs do not have any symptoms and they are detected only through examination of X-rays or ultrasound images of that location. Sometimes, there may be an occurrence of some symptoms like pulsing sensation, difficult in swallowing, pain, hoarseness or coughing. Pain is caused due to rupturing of the arterial wall or increase of loading on the arterial wall which may be very high. These types of diseases are detected only through physical examinations like computed tomography (CT), X-rays or ultrasonography, angiography and also by magnetic resonance imaging (MRI). Acquired CT scans are mainly helpful in precisely detecting the location and shape of the disease. The main causes of CVD include mainly atherosclerosis, syphilis, atheroma, congenital defects, obesity, smoking, hypertension, trauma,

hereditary conditions and as well as hemodynamic and arterial biomechanical factors. The research work of this thesis focuses mainly on treatments of arteries with atherosclerosis disease. Atherosclerosis is characterized by the accumulation of plaque formed from cells, lipids, connective tissue, calcium and other substances inside the inner lining of the arterial wall as shown in Figure 1 (B) which leads into narrowing of the arterial wall and abnormal blood flow [3].

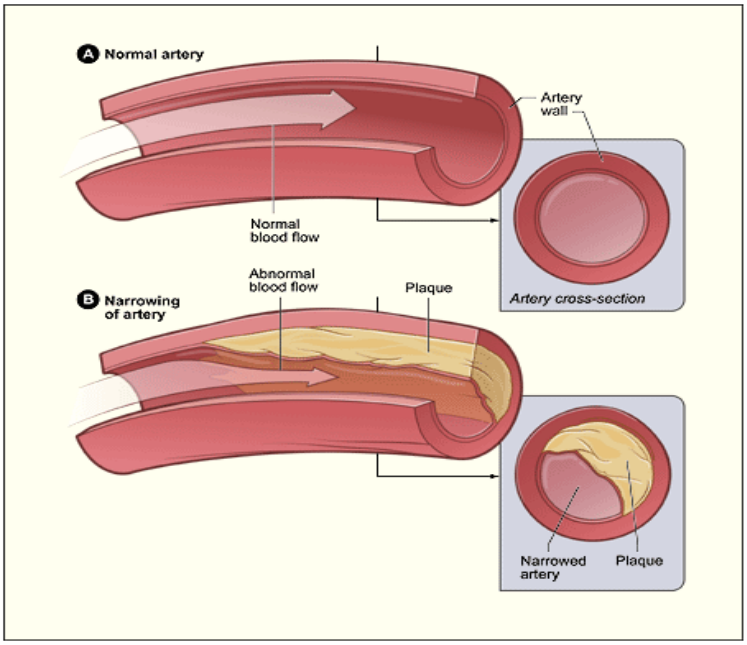

Figure 1 : Schematic representation of artery with atherosclerosis-plaque inside the arterial wall [3]

Atherosclerosis is a fairly common problem associated with aging. According to the University of Maryland Medical Center (UMMC), 80 to 90% of individuals over the age of 30 have some degree of atherosclerosis [4]. Atherosclerosis affects any artery in the body, including arteries in the heart, brain, arms, legs, pelvis and kidneys that lead to serious health complications, heart attack, stroke or even death [4, 5].

Arteries are the blood vessels that carry oxygen and nutrients from the heart to the rest of the body. The buildup of plaque hardens and narrows arteries. It limits the amount of flow of oxygen-rich blood to organs of the human body. Plaques from atherosclerosis can behave in

different ways [5]. Plaques may stay within the artery wall and grow to a certain size and stop. If the plaque invades the inner arterial wall less than 50% it may never cause symptoms. However, plaque can grow in a slow, controlled way and eventually cause significant blood flow obstruction which is approximately 50% or more blockage of the inner arterial wall . Pain on exertion (in the chest or legs) are the usual symptoms; the worst-case scenario consists of plaques that suddenly rupture, break and form blood clot inside an artery which can lead to thrombosis disease[5].

The first line of defense for this disease is prevention by taking some strategies such as following certain food regimes, exercises, avoid smoking and the like. However, sometimes it cannot be effective due to the advanced stages of atherosclerosis disease which are cured only by treatment. In addition to medications there are several types of surgical interventions as follows:

- Atherectomy is a minimally invasive surgical method of removing plaque burden within the vessel as shown in Figure 2a [6].

- Balloon angioplasty an empty and collapsed balloon on a guide wire, known as a balloon catheter, is passed into the narrowed locations and then inflated to a fixed size using water pressures some 75 to 500 times normal blood pressure (6 to 20atmospheres). The balloon forces expansion of the inner white blood cell/clot plaque deposits and the surrounding muscular wall, opening up the blood vessel for improved flow, and the balloon is then deflated and withdrawn as shown in Figure 2b [6]. The treatment is being done by angioplasty, an invasive procedure where a balloon-tipped catheter is inserted into the narrowing and expanded which is also called stenosis. It helps in the widening of the vessel lumen and makes the flow of blood effective. By using this technique there are some complications like closing of the vessel after few days or weeks. In order to overcome problems during treatment a mesh tube called stent is used which is expandable and remains inside the vessel even after expanding and prevents the plaque from obstructing the artery.

- Stent angioplasty or stent implantation, a metallic mesh tube i.e. stent is mounted on a catheter and inserted into the blood vessel to counteract the effects associated with plaque growth inside the artery as shown in Figure 2c [6]. After being released by a delivery system (a system of catheter tubes), the stent self-expands, compresses the plaque and exerts a radial force on the blood vessel to keep it open.

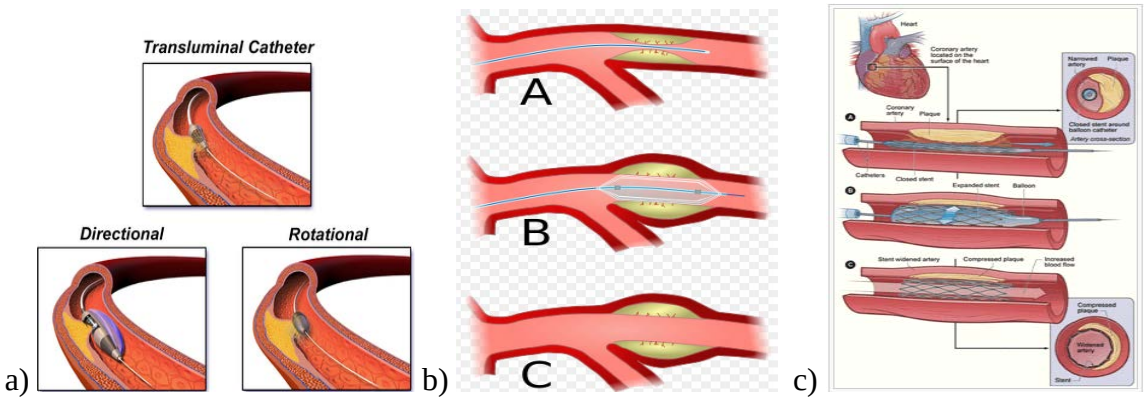

Figure 2: Surgical interventions for treating atherosclerosis diseases in arteries a) atherectomy b) balloon angioplasty c) stent angioplasty[6]

1.2 Types of Stents

There are different types of stents used such as bare-metal stent (BMS), a drug eluting stent (DES), a bio absorbable stent, a dual therapy stent (combination of both drug and bioengineered stent) [7,8,9].

1.2.1 Bare-Metal Stent (BMS)

A bare metal stent (see Figure 3) is a vascular stent without a coating of drug (generally used in drug-eluting stents). It looks like a mesh tube of thin wire. Bare metal stents are the ones used in the cases of cardiac arteries and are often made from 316 L stainless steel. Metal stents have a tubular lattice structure and can be assembled from a range of metals like NiTinol, stainless

steel and cobalt chromium. Ideally it should be flexible and spring-like, conforming to the shape of the arterial wall.

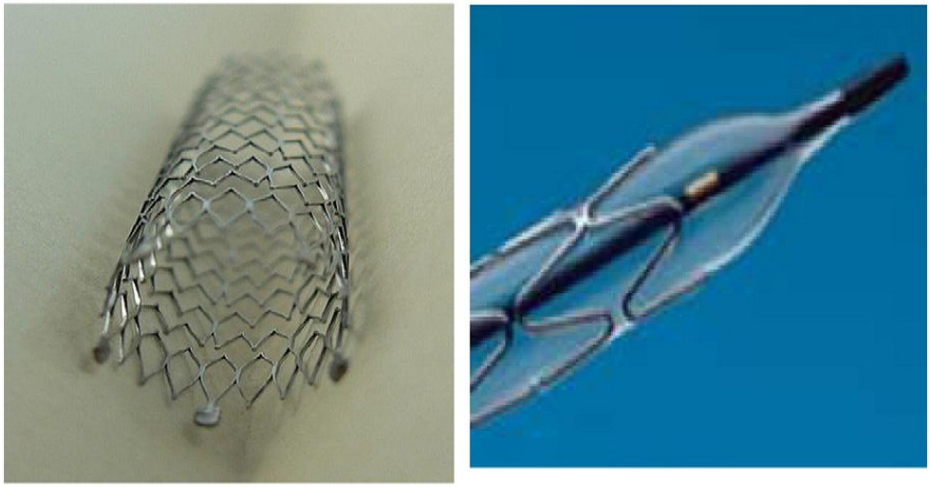

Figure 3: Left: BMS stent, Right: BMS stent with inflated balloon [7, 10]

The goal is to hold the inner wall in its newly compressed position without changing the diameter. The diameter of the stents can range from 2mm to 4mm depending upon the vessel size, condition and the type of disease. The length ranges from 8mm-38mm depending upon the length of the atherosclerosis in vessel. The materials differ in degrees of strength and flexibility. According to engineers, specific material and designs can create greater resistance to stent fracture and also these materials are radiopaque and biocompatible. Radiopaque helps the physicians in visualizing the stent while implanting by using a fluoroscope. For example, cobalt chromium stent material is more radiopaque and durable than stainless steel. Manufacturers are also introducing lot of designs like multicellular corrugated, coil and serpentine. Some of these designs are included with a lining of carbon, platinum and heparin in order to decrease the potential of thrombosis [7-10]. One disadvantage of using BMS in the past was occurrence of restenosis which means recurrence of stenosis i.e. renarrowing of the blood vessel. In the recent years, usage of bare metal stents has also decreased the elastic recoil effect after the balloon angioplasty surgery. Thereby the incidence

of restenosis has been dropped to around 25% within the 3 to 6 months after the surgery. However, stents fracture laterally because of the biomechanical environment of the vessels. Mainly stents in patients with peripheral artery disease (PAD) where there is a movement like sitting, running, walking and standing are associated with stent fracturing. Stent fracture rate has been approximated to around 50% in patients with PAD and thereby leading to restenosis [11].

1.2.2 Drug-Eluting Stent (DES)

A drug eluting stent (see Figure 4) is a stent placed mainly in the narrowed, diseased peripheral and coronary arteries that slowly releases a drug to block cell proliferation and heal the traumatized area in the vessel. This prevents restenosis [7-10].

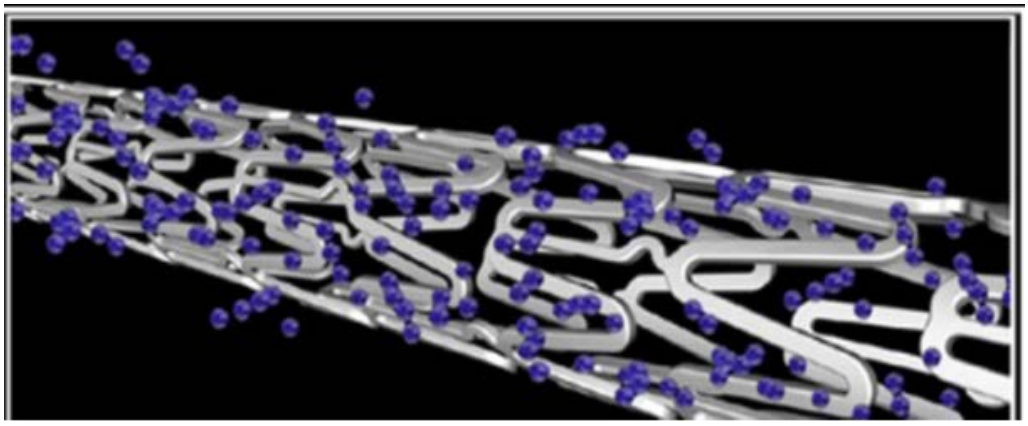

Figure 4: Drug eluting stent [10]

The Food and Drug Administration (FDA) has approved DES after clinical trials showing superior performance to BMS to treat narrow arteries and decreased number of major adverse cardiac events (MACE). MACE is generally defined as death, myocardial infarction, or the need for a repeated revascularization procedures. DES consists of three parts:

- Stent platform: The basic stent platform is the BMS which has expansion, flexibility and radiopaque. Cobalt chrome alloy is stronger, thinner and more radiolucent and it is less

allergenic. Mostly DES is based upon the BMS [7, 10].

- Coating: Typically it is a polymer which holds and releases the drug into the arterial wall by contact. Primarily they were few durable coatings which are been replaced by new coatings that are biodegradable after the drug has been released as shown in Figure 5 [9].

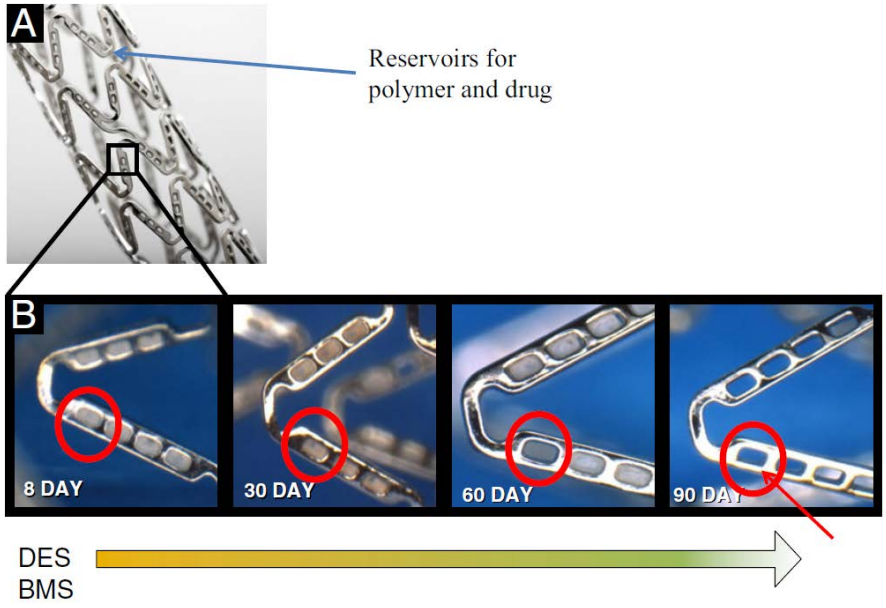

Figure 5: a) The NEVO cobalt chromium stent, which has an open-cell design and unique reservoirs that contain a biodegradable polymer and sirolimus mix that b) completely biodegrades within 90 days [9]

These coatings are generally dip coated or spray coated. There can be one or more layers depending upon the requirement. For example the first layer for adhesion, next layer for holding the drug and third coat can be to slow down the release of the drug and increase its effectiveness [7, 10].

- Drug: As explained above the drugs function is to mainly inhibit the neointimal growth and suppress the cause of restenosis. Neointimal hyperplasia is the proliferation of the smooth muscle cells during the inflammation of the balloon. Hence in order to suppress this growth immunosuppressive and antiproliferative drugs are used. Drugs like sirolimus and paclitaxel were

been used primarily but now new drugs are being used in order to prevent current problems [7, 10].

-

1.2.3 Biodegradable Stent (BDS)

The structure and geometry of BMS and DES are resembled for these stents, but they are made of material that the body resorbs after certain amount of time anywhere from 3 months up to 2 year. From some researchers' perspectives, fully BDS (Figure 6) is superior to conventional bare or drug-coated metallic stents in terms of drug elution and vessel scaffolding, which are only provided by the stent until the vessel has healed. Then nonendothelialized stent struts, or drug polymers can exist for long term following stent thrombosis reduced dramatically [9].

a) 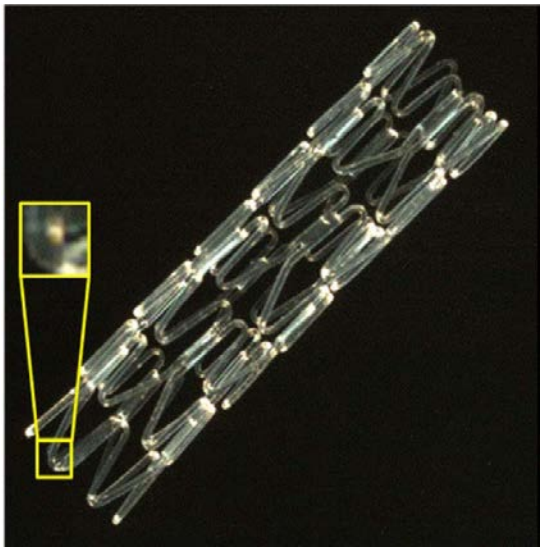

b) 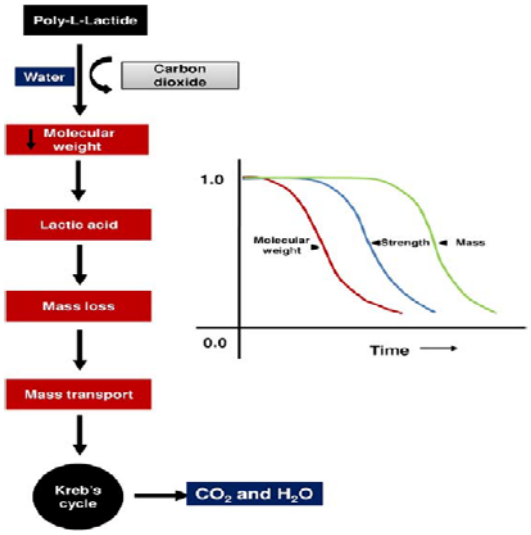

Figure 6: a) The Igaki-Tamai BDS stent with gold markers b) metabolism cycle of PLLA[9]

Physiologically, the absence of a rigid metallic casing can facilitate the return of vessel vasomotion, adaptive shear stress, late luminal enlargement, and late expansive remodeling. On the other hand, BDS dismiss some patients' doubt on "an implant in their bodies for the rest of their lives" [10, 12].

Currently the avaiable BDS can be manufactured by numerous type polymers polymer alloy (Figure 6 a) according to different chemical compositions and subsequent bioabsorption time. Among them, poly-lactic–acid (PLLA) is widely used as prominent material in numerous clinical implantations, i.e. soft-tissue, orthopedic implants, and resorbable sutures [10, 12]. Another material is PLLA, it is metabolized via a period of one to one and a half yesrs of Krebs cycle into inert particles of carbon dioxide and water as phagocytized by macrophages (Figure 6 b) [9, 13].

Although BDS being a promising stent, researchers have to face these problems: the polymer lacks radio-opactiy to be the backbone to a coronary stent, compared with stainless steel, reduced radial force reduced weaken the ability of the stents deformation. Even if these BDS stents show impressive results, such as minimal thrombosis, moderate intimal hyperplasia, and a limited inflammatory response, however, it is still hard to develop the manufacturing technology [9, 14, 15].

A tremendous amount of stents have been reviewed and implemented into patient care and a summary of stent types sold on different markets is listed in Table 1 [8, 9, 16]. Those parameters including material, form, fabrication, geometry and type of coatings can influence the stent performance. Figure 7 summarizes varieties of combination of these parameters. Stent design can be mesh structure, coil, slotted tube, ring, or multi-design. Laser machining is the most common technique for fabricating stents but photochemical etching, EDM, and water-jet cutting are other methods used [17]. Based on the stent design and characteristics desired the most suitable fabrication technique is selected. Figure 7 summarizes different parameters and techniques for stents fabrication.

Table 1: Summary of Current Stents Used Worldwide

Stent Type	Sold on the Market	Companies	Stent platform Material	Name	Drug eluting time	Location used
Metallic stents with durable polymers coating	4	Medtronic, Boston Scientific, Elixir Medical	Cobalt chromium, or platinum chromium	Endeavor Resolute(ZES), Elixir DESyne, TAXUS Element(PES), PROMU	< 90 days	USA
Metallic stents with biodegradable polymers coating	12	Sahajanand Medical, JW Medical System, Cordis, Biosensors, Terumo,Devax Inc, OrbusNEich, Boston Scientific, Elixir Medical, Xtent	Cobalt chromium, platinum chromium, stainless steel, or nitinol	XTENT, SYNERGY, Combo, NEVO, Biomatrix, NOBORI	<90 days	all
Polymer free metallic stent	4	Minvasys, Biosensors, MIV Therapeutics, Translumina	Cobalt chromium, or stainless steel	AmazoniaPax, BioFREEDOM, VESTAsync, Yukon	Avg. of 30 days	all
Metallic stents coating	12	OrbusNeich, Medtronic, Sahajanand Medical, Hexacath, Abbott Vascular	Cobalt chromium, or stainless steel	Genous Stent, R-stent, Blazer, Azule, Cornnium, Catania	N/A it is Bare Metal Stent	all
Biodegradable	10	OrbusNeich, Kyoto Medical JP, REVA Medical, AbbottVascular, Biotronik	Poly-L-lactic acid, 3Xlactide polymers, Tyrosine-derived polycarbonate, Polymer+salicylate, Magnesium alloy	Igaki-Tamai, BVS, REVA, IDEAL, AMS	4-36 months absorption time	all
Bifurcation(Ball oon expandable)	10	TriReme Medical, Invatec, Abbott Vascular, Minvasys, Boston Scientific, Tryton Medical	Cobalt chromium, or stainless steel	Antares, Ivatec TwinRail, Tryton, Petal, Niloe Croco	N/A	all
Self-expanding	5	Devax, Cappella, Stentys	nitinol	Axxess, Sigeguard,Boston Scientific	N/A	all

Figure 7: Stent fabrication techniques

However, despite the advancement in stents and the variety of stents available, restenosis (i.e. reoccurrence of restricted blood flow) still occurs in patients with 50% stent failure rate [11, 18 -20].

1.3 Basic Stent Characteristics

Stents are designed with a succession of rings and connectors. Rings or hoops (Figure 8a) provide radial support, and connectors (Figure 8b) hold rings together contributing to longitudinal stability. Number of crowns, strut (figure 8c), and connector structure define each stent design and its mechanical characteristics [21]. The number of crowns and cells change at different diameter with respect to the size of the vessel. For large vessels typical stent diameter is 3.5 – 4 mm and for small vessels the typical stent diameter is 2.5 – 3 mm. Several variations of stent designs are given in Figure 9.

a) 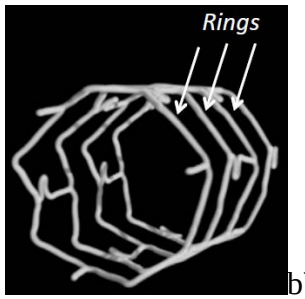

b) 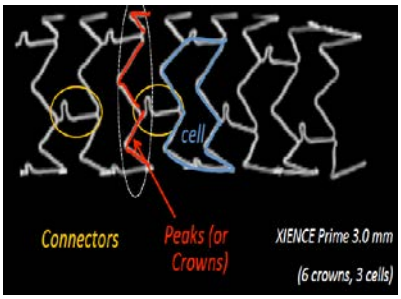

c) 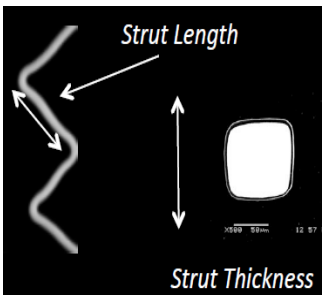

Figure 8: Stent geometry germinology a) rings (hoops) b) connectors c) strut dimensions [21]

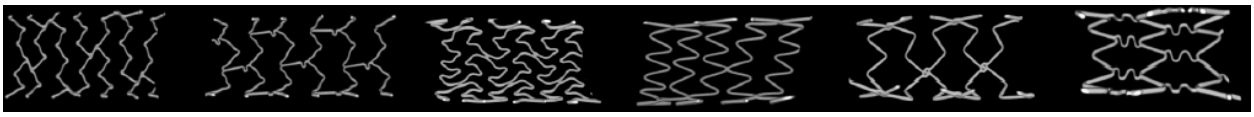

Figure 9: Various stent designs [21]

1.4 Arterial Structure and Classification of Arteries

All blood vessels consist of three distinct layers or tunicae: the tunica intima, tunica media and tunica adventitia (Figure 10) [22].

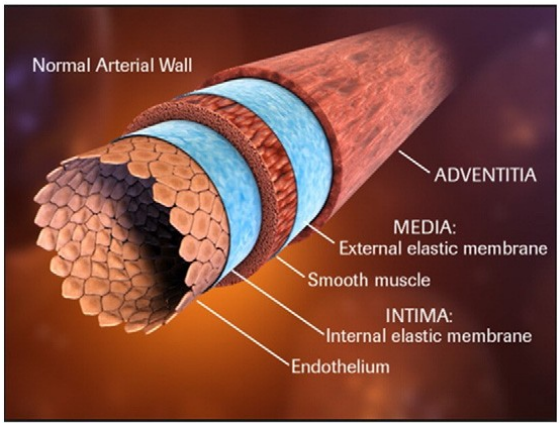

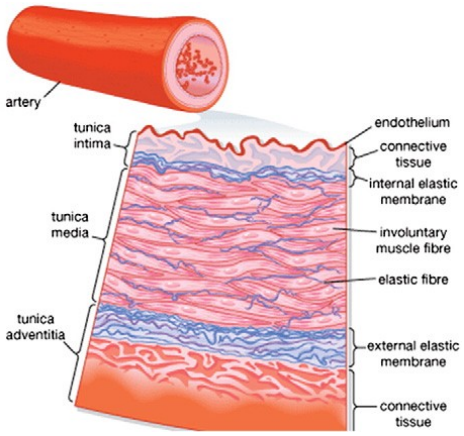

Figure 10: Schematic representation of distinct layers of arterial wall Left: top view of layers in arterial wall [23] Right: cross-sectional view of layers in arterial wall [24].

The intima is a thin endothelial layer that lines the inside walls, and sits on a very thin (~80nm) basal lamina of a net-like type IV collagen in young human. Endothelial cells, typically elongated in the direction of the blood flow, act as a semipermeable membrane, through which

nutrients and chemical signals can reach the cells in the vessel wall from the bloodstream. The intima has also a key role in regulating the active response of the vessel through which pressure regulating agents reach the media. Additionally, in order to help control the vascular tone the intima produces NO (nitric oxide), which relaxes smooth muscle cells in the media. Despite its great functional importance, due to its small thickness in young arteries the intima is usually neglected when considering the different layer contributions to the global mechanical resistance of the vessel wall. A fenestrated sheet of elastin called internal elastic lamina separates the intima from media [22]. The media is formed primarily by smooth muscle cells (SMC) that are embedded in an extracellular plexus of elastin and collagen (mainly types I and III) and an aqueous ground substance that also contains proteoglycans. Depending on the internal arrangement of the smooth muscle cells in the media, it is distinguished between elastic arteries and muscular arteries. The former tend to be large-diameter vessels close to the heart, and include the aorta, the main pulmonary artery, the common carotid and common iliac arteries. Their most characteristic histological feature is the so-called lamellar unit, a sandwich-like ‘sublayer’ of smooth muscle cells and thin elastic laminae. Elastic arteries have concentric ring-like structures that are tied together by radially oriented collagen. In muscular arteries, the media appears as a single thick ring of smooth muscle cells. The SMC are embedded in a loose connective tissue matrix and arranged as a sequence of concentric layers of cells, which can reach numbers of 25–40 in larger vessels like in the femoral artery [22]. The adventitia is the outermost layer of the vessel wall. It consists of a dense network of type I collagen fibers with scattered fibroblasts, elastin and nerves. In medium and large arteries there is also the vasa vasorum, an intramural network of arterioles, capillaries and venules that supply large vessels where the distance from the main bloodstream to the outer sections of the wall does not allow for proper interchange of O2, CO2, nutrients and

metabolites. The presence of nerves in the adventitia allows innervation of smooth muscle in the outer media, via the diffusion of neurotransmitters. As for the fibroblasts, they are responsible for collagen production, particularly type I, and thus regulate the connective tissue. At higher pressures, the fibers gradually straighten, confirming the hypothesis that the adventitia serves as a protective sheath, preventing rupture of the vessel due to an acute increase in pressure [22].

Arteries classification - Generally, arteries are classified to elastic arteries (conducting arteries, including aorta, brachiocephalic, common carotid, subclavian, vertebral, pulmonary and common iliac) and muscular arteries (distributing arteries, including brachial artery, radial artery, popliteal, common hepatic artery) [22, 23]. Legs, arms, and lower body depend on the arteries to supply blood and oxygen to their tissues. Hardened arteries can cause circulation problems in these areas of the body. Coronary arteries are smaller and thinner arteries typically near the heart and the larger arteries are designated as peripheral with the largest artery in the body being the femoro-popliteal artery (FPA) with nearly 50cm in length that encompasses the superficial femoral artery (SFA) and popliteal artery (PA) as shown in Figure 11 [7, 15, 25].

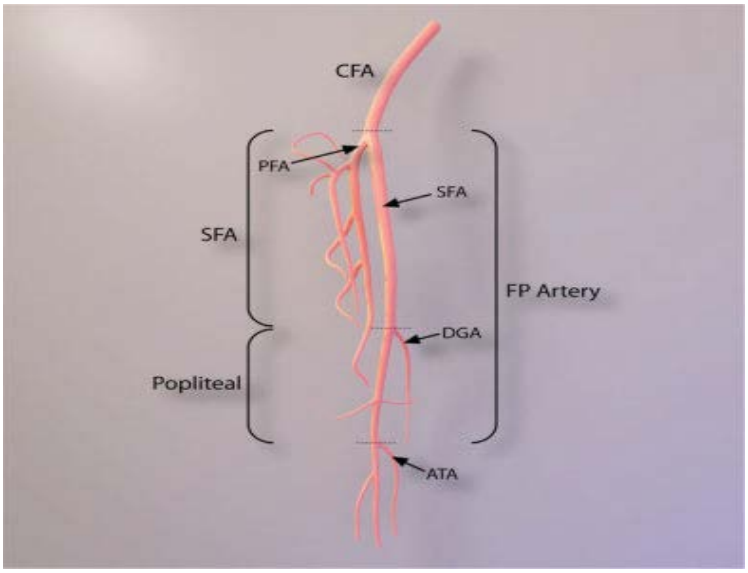

Figure 11: Anatomy of the femoropopliteal (FP) artery. CFA, common femoral artery; PFA, profunda femoral artery; SFA, superficial femoral artery; DGA, descending genicular artery; ATA, anterior tibial artery [15].

1.5 Atherosclerosis, Peripheral Arteries (PA) and Stents-Vessel Interaction

Although more is known about atherosclerosis in the general population specifically with coronary artery disease, not much is known about the cause and best management for peripheral artery disease (PAD) and thus PAD follows the same therapy protocols as for coronary artery disease. Especially, assessment and management of PAD in patients with diabetes mellitus are unclear and present special issues. When atherosclerotic plaque and blood clots reduce blood flow to the legs or, less often, to the arms, the condition is called peripheral artery disease (PAD) (Figure 12). PAD makes walking painful and slows injury healing. In the worst cases, it can result in the loss of a toe, foot, or leg.

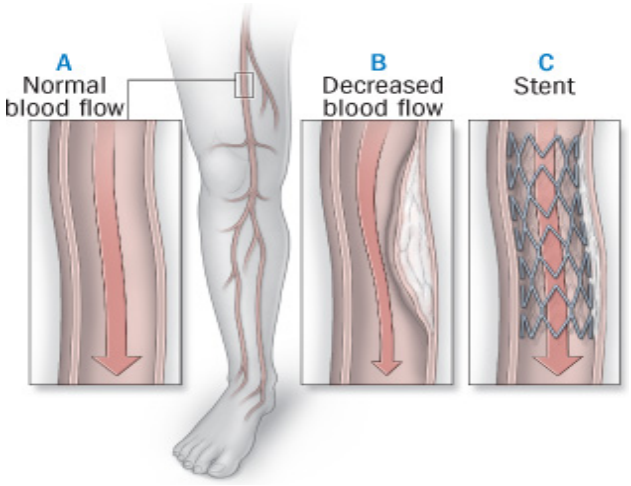

Figure 12: Blood flows through a normal artery (A). In peripheral artery disease, atherosclerotic plaque narrows the artery and impedes blood flow (B). During angioplasty to restore blood flow, a stent maybe inserted to keep the artery open (C). Stent implant restores normal blood flow [26]

Atherosclerosis appears preferentially at sites of complex geometry e.g., along the outer portions of the bifurcation in artery and only within specific points within the vessel. During every day body function, parts of the legs are exposed to multiaxial deformations with up to 60% rotation and 20% contraction as the leg is bent from an extended position [27]. As a result, stent deployed

in the intersection of the femoral and popliteal arteries is exposed to significant multiaxial displacements due to the musculoskeletal motion as well as bending, torsion, flexure, tension, and compression (Figure 13 left) [15, 28]. It is also known that stent implantation leads to artery strengthening opposed to natural artery curvature which can lead to various wall stresses and hemodynamics changes within the implantation region (Figure 13 left and right) [16].

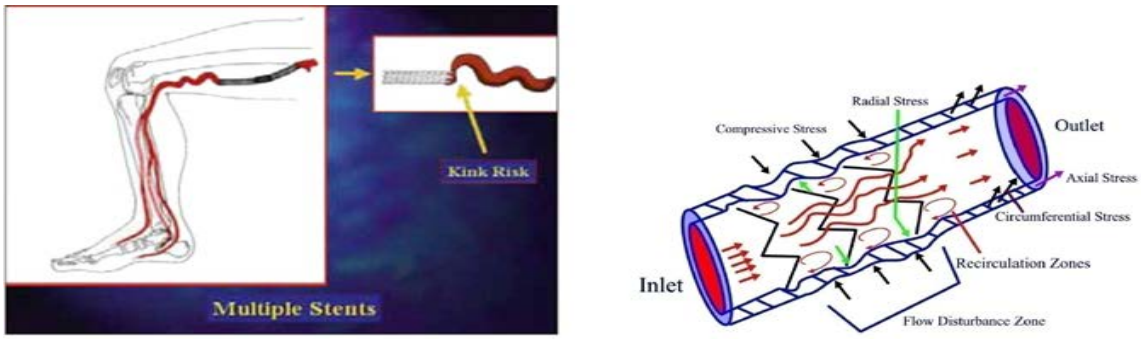

Figure 13: left: As stents are placed into the artery, the artery ability to bend and compress is reduced. The adjacent unstented artery bends more, possibly resulting in kinking at the margin of the stent [28]; right: Stenting leads to different wall stresses and hemodynamics within the implantation region [16].

The stated issues can lead to fracture of the stent in this region, which has been directly linked to in-stent restenosis issues. Several advance technologies such as: doppler ultrasound, magnetic resonance angiography, and computed tomography angiography provide detailed image of the stented arteries with quantitative characterization of the disease where doppler ultrasound also provides information on blood-flow velocity and turbulence [29]. It has been shown that several mechanical factors such as pulsatile or steady blood flow velocity and the corresponding wall shear stress in the coronary artery can lead to cell remodeling and decrease of mechanical strength in the arterial wall [30, 31]. These factors lead to specific alternating and steady stress state in the arterial wall such as elongation, compression, bending, tortuosity and the like that produce a fatigued environment. Especially, in PAD patients who in addition to internal factors, have external factors by using their legs while walking, climbing, seating down, standing up also

contribute to increase of stress-strain state in the artery carrying the stent implant. Further, in addition to imposed stress-strain state Berry *et al*. 2002 [31] show stented arteries also have a mechanical mismatch at the interface between the arterial luminal wall and the stent. This mismatch between stent and artery leads to the development of circumferential stresses, causing vascular stretch, and changes in hemodynamics [31] as shown in Figure 13. These issues branch this exciting area of research into two directions: understating the biomechanical state of the artery and mechanical properties and deformation that the stent undergoes under the influence of the arterial forces. Literature reports show that the biomechanical behavior of the arterial wall can be, and has been indirectly described, utilizing computational fluid dynamics (CFD) analysis to quantify the variation of wall shear stress of the contained blood flow [32]. Experimental flow visualization analysis of coronary vessels has also been performed, by various imaging of infused particles; this has been particularly illuminating and important in bifurcating regions since these zones have high probability for plaque accumulation [16]. Further, CFD has been used to characterize wall shear stress development for canine femoral arteries, using non-Newtonian simulation models, analyzing resultant changes in blood flow velocity, and wall shear stresses on the sensitive endothelial cell layer, and also the role of incorporated stents in regulating shear development in these regions was demonstrated [33]. Finite element analysis has been used to simulate and apply many features to the stent design such as: smaller size, balloon crimping characteristics, flexibility during navigation, less recoil following expansion, and improved reliability. FEA offers means of not only analyzing stent mechanics but also the interaction of the stent with the arterial vessel, stent induced vessel injury, as well as stent fatigue over time [34 - 39]. Most important, FEA modeling can provide a method to evaluate and quantify mechanical derangements, thus to determine the potential “risk” regions for high stress formation within the

plaque and artery, including the role of stent contact in modulating these effects. However, up to date studies are mostly focused on the coronary arterial bed and its hemodynamics after arterial stenting. Literature reports studies on the topics of SFA and popliteal artery (PA) stenting (Figure 11) [40-62], but peripheral stenting, specifically SFA with high stent failure rates is a less studied field. Recent literature review on this topic summarizes heterogeneous study designs that include different physiologic settings from young to mature participants and with and without disease, and cadavers which produced results specific to anatomic location within the SFA/PA [62, 63]. Further, a compilation of stent improvements for treating atherosclerosis in SFA/PA shows evidence of increased durability, finer surface finishes, increased flexibility, and longer lengths. Yet stents still fracture at measurable rate and clinical significance of stent fracture remains controversial. A direct causal relationship between stent fracture and clinical outcomes, such as restenosis, has not been established ; however, what is clear is the uniqueness of the biomechanical environment of the SFA compared to other vascular beds [62]. Stent desired characteristics include: flexibility, trackability, high radial strength, circumferential coverage, low surface area, and hydrodynamic compatibility [64]. Each reported stent design has advantages and disadvantages but no stent incorporates all of the cited characteristics. In other words there is no ideal stent however, if one quantifies the mechanical behavior of stents with their specific characteristics and match with the diseased artery conditions there is no need for a standard off-the shelf ideal stent because, stent will be able to sustain this biomechanical artery environment for each patient individually that will lead to improved personalized treatments for patients with PAD and reduced stent failures especially cases that lead to death. Therefore, the main goal of this thesis is to quantify mechanical characteristics of specific stents using theoretical and computational approach.

In this thesis, Chapter 2 introduces theoretical and computational approach of stent linear analysis and nonlinear analysis, respectively. In Chapter 3, the properties of stent structure relates to geometric parameter is studied by means of theoretical and computational approach. Then, Chapter 4 list nonlinear analysis results of stent under expanding situation of deployment. Finally, in the last Chapter 5, conclusion of this thesis is listed and future work is discussed as well.

CHAPTER 2

THEORETICAL AND COMPUTATIONAL APPROACH

2.1 Theoretical Approach for Linear Stent Analysis

The high failure rate of stents used in patients with peripheral artery diseases [11] has lead researchers to give special attention towards analyzing stent structure and characteristics. Though many different stent structures with special units have been evaluated previously [65], the fundamental understanding between stent design and its performance is still inadequate and incomplete. Generally stent design be viewed as a series of deforming beams, wrapped into a cylindrical shape like a spring. Some popular structural mechanics formulas [66, 67] can be used to relate deflections of beams to stresses, strains, and forces. During the research of stent structure, mechanical principles closely connected with stent design inputs, such as diameter, wall thickness, and strut length, to perform outputs as strength, surface area, mass, contact pressure, and strain. These relationships are fundamentally instructive for stents fabricated from steel or super-elastic nitinol, which reach strains of 1-2% with a substantially linear elastic relationship to stress. Nitinol is particularly well suited for analysis because this is an order of magnitude higher than conventional engineering materials[65].

The mechanical properties of stents are usually described according to the theory of elasto-plasticity, which characterizes deformation of materials as a function of the applied load [66]. For example, a beam of length l deforming under flexure force can be viewed as a cantilever beam loaded at one end and fixed at the other end. Then the deflection (δ)at the fixed end is calculated by equation (2.1):

$$\delta = \frac{Ml^2}{12E_sI} \tag{2.1}$$

M is the applied moment, $I = \frac{tb^3}{12}$ is the second moment of area of the beam with t being the thickness of the beam and b being width of the beam [66, 67]. The extension of a beam due to the axial force F enforcing on the ends leads to modified equation (2.2) for deflection:

$$\delta = \frac{Fl}{btE_s} \tag{2.2}$$

In cases under large loading resulting in plastic deformation, such as the stent that undergoes full expansion from its initial state by means of balloon inflation, stents take irreversible breakage of bonds and the formation of dislocations and slip planes (Figure 14) .

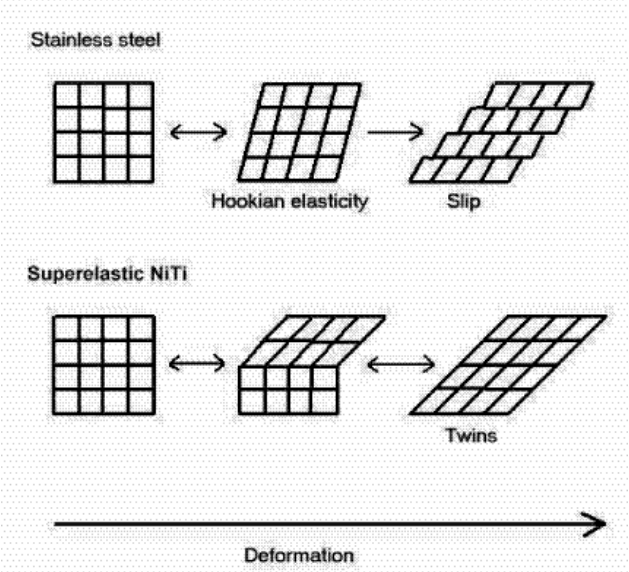

Figure 14: Deformation of different materials under large loading

While in relatively small loading case, the stent behaves as a linearly elastic structure: after removing the load, the stent assumes its original configuration. The response of the stent to small loads within the region of linear elasticity is the basic type of stent behavior. In this case, the mechanical properties of an isotropic material are characterized by Young's modulus (E), which represents the stiffness (ε) of an elastic solid (i.e. stent struts), and by Poisson's ratio (ν), which represents the compressibility of an elastic solid (stent struts) [66]. In this thesis the behavior for

commercial stents is investigated by analyzing the special stent structure combining geometric factors with the material factors in the small deformations exhibited by an already expanded stent inside the artery for which, linear elasticity might be an adequate consideration at the initial stage of this study. The next stage is study of the large deformations that a stent undergoes during balloon expansion by considering both nonlinear elasticity and plasticity and discussing more applicable design parameters of the stent design.

2.2 Numerical Approach for Linear and Nonlinear Stent Analysis

When delivered to a region of complex vessel anatomy, the medical devices such as the stents can create and experience a complex dynamic situation. Finite element analysis and numerical simulation tests are increasingly important for the design and development of medical devices (i.e. stents) in order to shorten the stent development time to market and improve patient care. The possibilities of finite element analysis (FEA) and computational fluid dynamics (CFD), combined with contemporary imaging techniques, greatly facilitate stent research. In order to create realistic computational models to perform this research, the geometry of the stent in question and its delivery system should be very accurate. Then, a shape design support system for stents is proposed considering well the production process of stents, shown in the frame of design support system to simulate and evaluate the process. Some manufacturers obtain accurate stent geometry by segmenting nano/micro-CT images, transforming micro-CT data and reconstructing them in 3D using the Mimics Innovation Suite [68]. Then, researchers could optimize the 3D model's mesh by means of automated re-mesh technology, which is instrumental in providing all necessary dimensions of the 3D structure to create approximate parametric models. This also plays a significant role in the future development of personalized stenting, thus improving the patient's

treatment. The Mimics software proved to be an excellent tool to get very precise geometry ready for virtual testing. Mimics accepts medical images such as CT, IVUS or MRI and allows the modeler to reconstruct the area of interest into 3D models (Figure 15) with the specific geometry then export them as typical IGES files ready to be analyzed in FEA/CFD packages (i.e. ABAQUS, ANSYS and ANSYS Fluent, COMSOL, NASTRAN and PATRAN) in order to support further finite element analysis (Figure 16) [68].

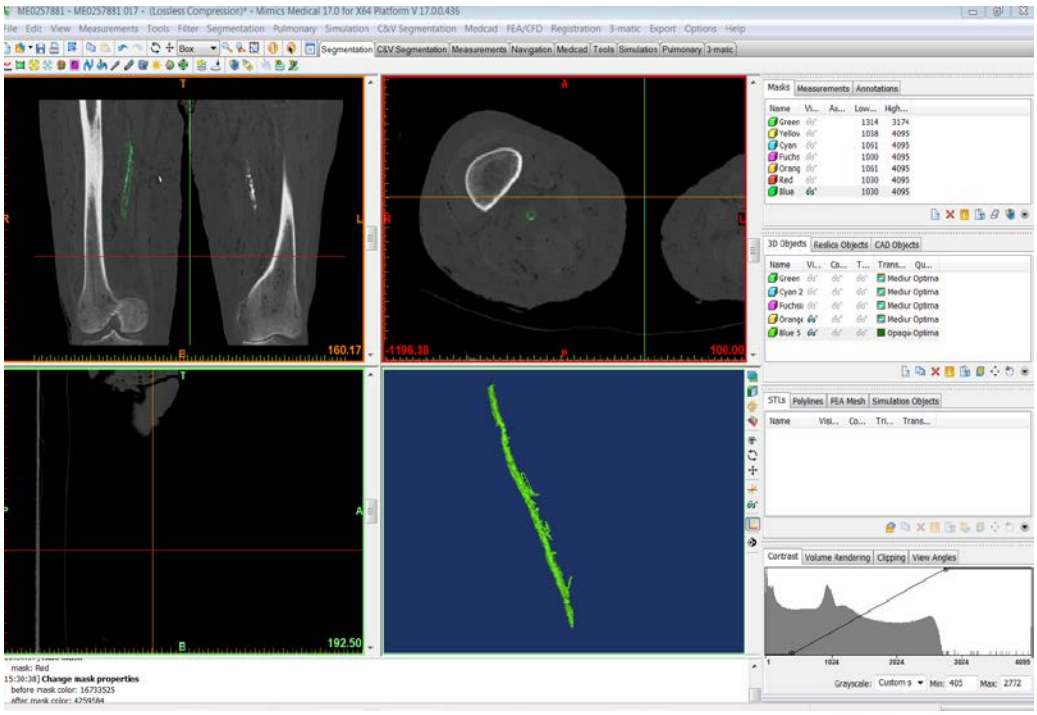

Figure 15: Schematic showing Mimics software reconstruing 3D image of an artery from CT scan [68]

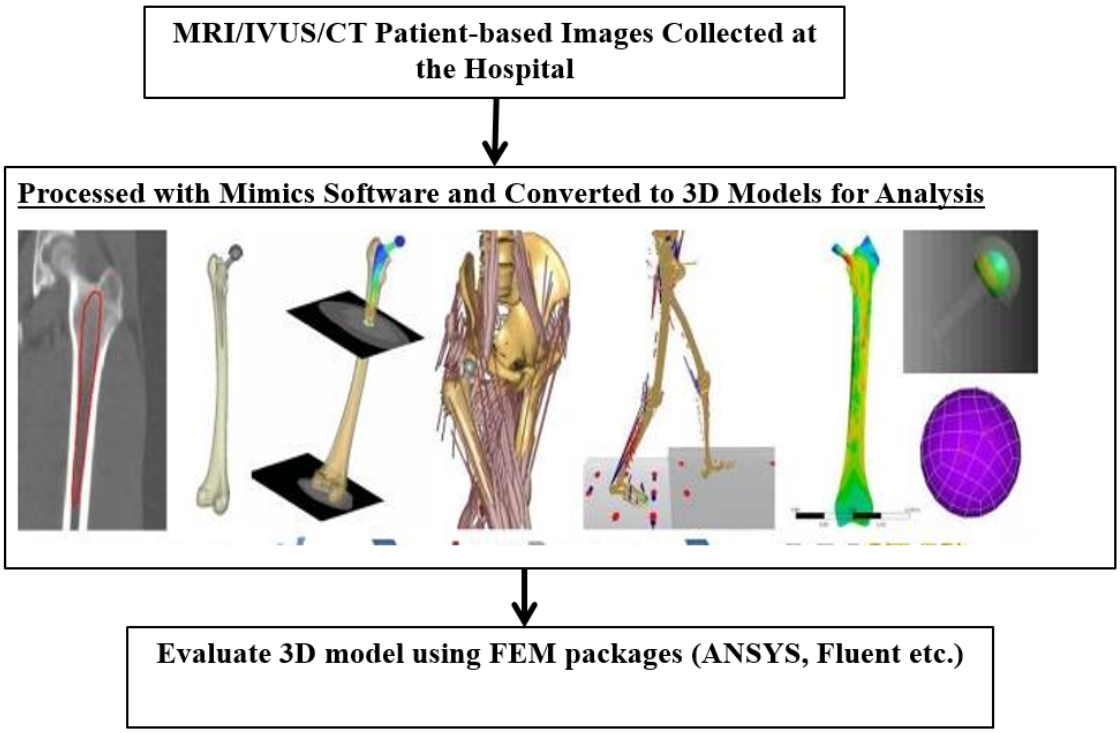

Figure 16: Flowchart showing step by step analysis of 3D models using medical images

Further, for most accurate results the first step in the numerical simulation is to analyze the stent properties as a whole before combining it with the artery model using principles of solid mechanics [67]. Some modeling software such as SolidWorks, NX, CATIA, and the like are powerful enough to model complex stent shapes. To complete the numerical analysis especially the nonlinear analysis, the finite element method requires a lot of information, including the geometry and the material properties of the stents, the effect of the catheter and the artery, and the accurate application of boundary and loading conditions. MSC Software allows for proper analysis of these inherently difficult (e.g. non-homogeneous, non-linear) research models [69]. In this thesis we use MSC Software to validate the linear deformation of specific stent designs previously analyzed theoretically and to simulate nonlinear deformation behavior of the stent using appropriate finite element models developed in Patran and solved with NASTRAN [70].

In the stent model, the stent geometry consists of several rows of identical geometry, one intermediate row at each end (the same geometry, but different strut width), and one final row at each end that has the same basic geometry (and increased strut width) with the exception that there is no 'connector' on the outboard ends (as there are no additional rows to be attached to). The repetitive nature of the geometry allows for a theoretical model or a finite element model of a portion of the entire stent to accurately characterize the stress state within the entire stent. This approach allows the finite element mesh to be finer in the region that is modeled, as opposed to using a similar number of elements for an entire stent, and therefore achieve an increase in accuracy while still characterizing the entire stent.

Generally, the popular stent is stainless steel or cobalt chromium alloy with characteristics of work hardening. Taking the cobalt chromium alloy into account, it can be viewed as a linear elastic material up to yield point, beyond the material yield point, time independent plastic behavior is prominent if assuming it without orthotropic or anisotropic effects. A Von Mises yield condition, commonly used with metallic alloys, along with a kinematic hardening law are used in the analysis.

When the material is strained beyond the yield point, the yield surface must change for continued strain hardening. The kinematic hardening law is used for the analysis herein, to take into account the Bauschinger effect presents during reversal of the stress field which occurs between the compression and inflation stages. Bauschinger effect describes that pre-straining in any direction, as defined by the principal axis of the strain tensor, will introduce an anisotropy for further deformation in any other direction [71]. The intensity of this prestrain-associated anisotropy is at maximum when the direction of further straining is opposite to that of the prestrain. A finite element test model was created in order to verify that the elastic-plastic material model

used in the analysis accurately represents the supplied material data. Generally, inflation of the stent may be performed using direct pressure applied to inside diameter of the stent or manually expanding the stent through prescribed boundary conditions. Attempts to inflate the stent with direct pressure can prove difficult due to the lack of geometric symmetry in the design and could result in unrealistic deformations of the stent. Consequently, the stent was set to reach the desired diameter, the stent shows elastic recoil.

The stent inflation analysis involves large deformations and large strains. The nonlinear material properties must be considered to accurately capture the deformation process. Therefore, the Lagrangian and the Eulerian descriptions are considered for the large deformations of the stents. The Lagrangian or material approach uses the initial configuration to describe the deformation whereas the Eulerian or spatial description uses the deformed configuration to describe the deformation, specially Lagrangian approach is used for elasticity effects.

Next, the total Lagrangian and the updated Lagrangian method are considered with respect to the un-deformed configuration. In this case, the inflation of the stent is modeled using an elastic-plastic material model, inelastic strains, which cause large deformations. Therefore, the updated Lagrangian method is used in the frame due to the inelastic deformations, then true (Cauchy) stress and true (logarithmic) strain are chosen to measure stress and strain. While the engineering stress-strain is to measure stress-strain data and ultimate strength. On the other hand, it is hard to relate true stress and true strain measures to their respective engineering stresses and strains under multi-axis stress state. therefore, equivalent stress and equivalent strain are the important quantities to the analyzed values.

2.3 Modeling of Stent Behavior Inside the Arteries – Loading and Boundary Conditions

Prevalent stents have numerous design patterns for the structure, the widespread interest focused on the properties of stent designs in terms of multiple types geometry [7-9]. By using bi-planar fluoroscopy for the generation of 3D models of stent geometry for assessment of stent fracture risk, some key factors of stent design had been studied, the measurement of strut length, separation angle and cell asymmetry are crucial to the whole stent design. Literature reports a quantitative assessment of the magnitude of uncertainty in the measurement of geometric parameters derived from 3D stent geometry in lieu of numerical simulation approach [72].

In order to optimize clinical performance and minimize negative effects, stent design plays a vital role. Several variables of design parameters are closely associated with the optimization of stent structure. Strut spacing, axial amplitude and radius of curvature were chosen as, showing good optimization results in terms of reducing stress in the artery wall [72, 73]

Most commercial stents were uniformly expanded from their crimping diameters such as 1.2 mm for PS and Express stents, 1.42 mm for Multilink-Vision stent, to 3.0 mm with 50% stenosis inside artery [73]. The stent designs caused deviations in arterial stress. On the arterial wall, the Von Mises stresses are higher at the proximal region of the plaque [74]. While all stents were subjected to the same linear ramping displacement, the maximum principal strain rate (strain as a function of time) on the stented arterial wall are apparently different. Moreover, with expanding to the 3 mm diameter, various stents induced higher different stresses over larger areas of the arterial wall. The elevated stress region largely depends on the strut shape of stents in terms of mechanical stress corresponding to the clinical observations [72, 73].

When crimping stents be placed in the exact location, the stents self-expand and exert a radial force on the blood vessel to keep it open. Once delivered, the response to blood pressure

(cyclic pulsating load) determines the fatigue life of the stent. Self-expanding stents have proven to reduce the extent of arterial recoil and restenosis as compared to balloon angioplasty procedures and provide a less invasive alternative in the treatment of endovascular disease [75]. After stent implantation, changes in the native vascular geometry may increase the risk of in-stent restenosis due to alternations in vessel wall compliance and subsequent changes in shear stresses, the implantation of rigid stents may cause flexion or hinge points in terms of the abrupt changes in vessel wall rigidity at the ends of stents. These hinge points have been associated with increased rates of restenosis and may increase the risk of edge dissection. Even in an era of drug-eluting tents which have reduced the incidence of restenosis, attention need to be given on the effects of stent induced conformational changes according to the SIRIUS trial results that restenosis occurred more commonly in the proximal peri-stent region than within or distal to the stent [16]. Figure 13 (right) shows typical loading conditions around the stent once inside the artery upon expansion.

When delivered to a region of complex vessel anatomy, the stent may have unfavorable effects on the flow dynamics (Figure 13 right). The axial stress, circumstantial stress and radial stress are present while the various anatomical bending are considered. The artery wall pressure depends on the blood properties. Arterial pressure of the systemic circulation in terms of the systolic pressure over diastolic pressure is represented as compressive stress [76]. Then it is possible to analyze the fluid zones, such as recirculation zones and flow disturbance zones considering the arterial pressure, blood viscosity, the density of whole blood, the pressure difference between vessel inlet and outlet with some assumptions like non-Newtonian flow etc.

In the femoropopliteal artery (FPA) mentioned before, the placement of stents is associated with high rates of stent fracture [62]. FP artery is subjected to significant biomechanical forces during leg movement. The primary components are axial compression, bending, and twist,

reflected by changes in length, curvature, and twist angle, respectively. The short term reported data provides an assessment of the magnitude of the alternations in these parameters in patients with peripheral artery disease. Length change, torsion, twist angle and flexion points/angles of SFA, PA and FA artery effectively quantify the realistic situation. The significant variation in the magnitude of these parameters along the length of the FP artery (e.g., curvature) and inter-patient variability (e.g., length) reflect the real boundary conditions and loading forces for analysis of the stent in FPA. Based on the FP artery 3-D models generated from patient medical images in different positions show significant changes in length, curvature, and twist in the PA and less pronaunced changes in length occur in the SFA (Figure 17).. Those conclusions contribute to the analysis of FP stents and promote the development of stents with reduced rates of stent fracture.

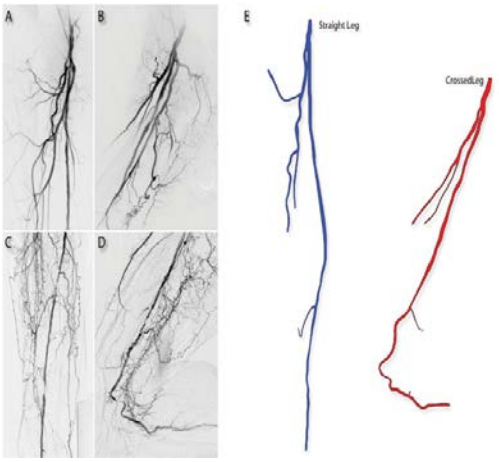

Figure 17: An example of a patient with significant conformational change in the popliteal artery segment [15]

In addition, poor performance of the intravascular device can result in undesirable clinical events such as thrombosis and intimal hyperplasia [77]. In order to minimize these adverse events, it is important to obtain a thorough understanding of the factors that contribute to an adverse outcome during the stent deployment process. Such device-related factors could include the stent

design and material as well as the deployment procedure. Characterizing some parameters of the stents: the deployment pressure which is required to achieve plastic deformation of the material beginning at the diameter of the crimped stent; the intrinsic elastic recoil by the elastic deformation of the material; the stent foreshortening and the stent coverage area by ratio between the area of the stent's external metal surface and the area of the arterial cylinder covered by the stent and the flexibility of the stent measured by the maximum radial displacement of the stent subjected to force.

The chapters that follow will lead us to step by step analysis and background theory of the development of each stent model and the linear and nonlinear analysis. In addition, Figure 18 shows flowchart with overview of the model verification for this thesis.

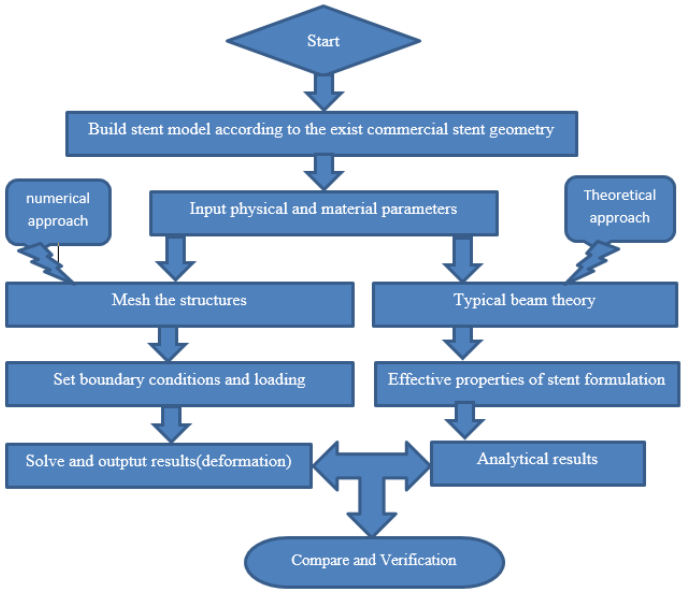

Figure 18: Flow chart with overview of the model verification

CHAPTER 3

THEORETICAL AND COMPUTATIONAL APPROACH TO STUDY STENT MECHANICS

3.1 Objective

The present investigation builds upon prior works and develops a theoretical model for predicting the elastic constants of general cell unit like rhombus shape on the mechanical behavior of the structure, including flexure and stretching and combination of these two conditions. The model had been considered both material properties and non-material properties (based on the structure geometric parameters), and then, derived the effective Young's modulus in two directions theoretically. In addition, depending on the geometry of the model, we compared the effective theoretical Young's modulus with equivalent results from the numerical FEA model and verify the validation of theoretical evaluation.

Mechanical Behavior under uniaxial and flexure loading of structure and the effect of geometric consideration on their mechanical properties were investigated by using finite element analysis and comparing with the numerical results.

3.2 Introduction

A cylindrical stent in arteries are subjected to significant mechanical loads from repetitive cyclical pressure loads and displacement of the artery wall as it expands and contracts slightly with each muscle spasmodic contraction in a long-term in-vivo service [78]. Though many different structures with special units have been evaluated in previous works, Karnessis et.al. studied the auxetic cellular models(Figure 19), its work evaluates mechanical properties of the structure via analytical approaches and verifies the influence of the geometric parameters; I.G. Masters and K.E. Evans cited honeycombs structure and developed the theoretical model to predict the elastic

constants of honeycombs by flexure, stretching and hinging[79]; Zahora et al.(2007) analyzed a woven spiral stent(Figure 20, left)[80]; Graeham et al.(2014) listed the hybrid unit structure stent[81]. Nasim Paryab et al.(2014) focused on helical stent(Figure 20, right) [82]; Alessio Meoli and Migliavacca et al.(2014) cited peripheral Nitinol stents[83]. However, the analysis of the other structural performance is still inadequate, such as the rhombus unit structure stent(Figure 21). Stents help prop the diseased arteries open and decrease the risk of blood blockage again, however, stents also enforce abnormally high stresses on arteries that can introduce adverse biologic response culminating in restenosis. Therefore, stents' strengths are key criteria for the biomedical device.

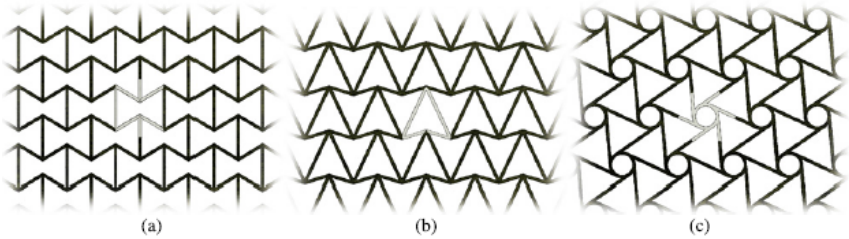

Figure 19: Inverted hexagonal honeycomb(a), V-type(b) and chiral(c) auxetic cellular structure in paper [76]

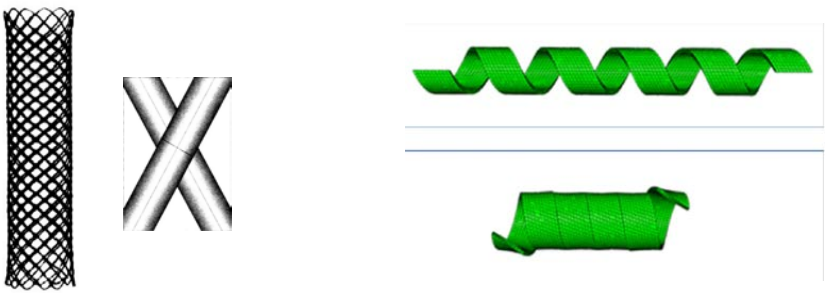

Figure 20: Left: Spiral stent with unwelded junction of two wires[80]; Right: helical stent[82]

This study focused on the stability behavior of generalized structure of stent (shown in Figure 21, Figure 22) and derives several property parameters relating to structure design. Two mechanisms can be identified by which struts can deform, namely flexure and stretching. Using

beam theory(Euler-Bernoulli beam Equation (2.1), Equation (2.2)) in mechanics each can be expressed mathematically. A rhombus structure (Figure. 22) was chosen in terms of its more common use and made by some main stream manufacturers. The stents are prone to fail by buckling under artery wall pressure, axial, circumstantial and radial loading in combination with various anatomical bending. The mechanical properties (Young's modulus in two main directions) of stent structures are derived by analytical approach. Figure 21 shows the scanning electron micrographs of stents with 8-strut (A) and 12-strut (B) designs after balloon expansion[84]. This expanded stent model has small deformation and the study starts with linear structural analysis.

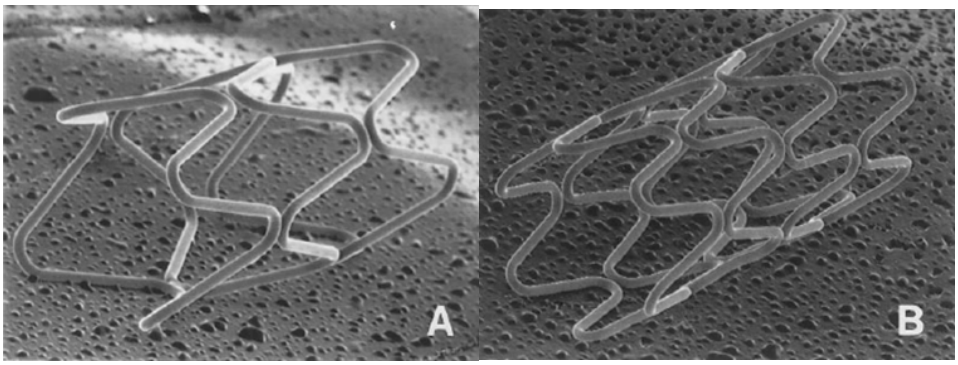

Figure 21: Scanning electron micrographs (magnificationX18) show stents of 8-strut (A) and 12-strut (B) designs after balloon expansion[84]

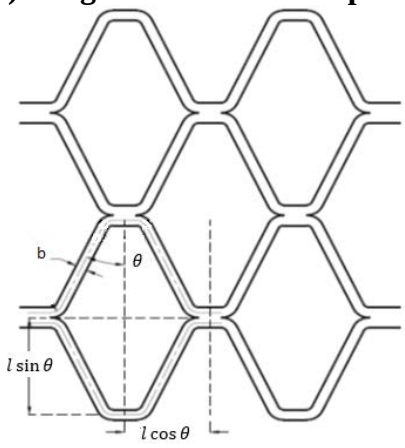

Figure 22: Stent structure includes arrangement of strut members

3.3 Approach

3.3.1 To Analyze the Effects of Geometric Parameters of Stent in the Artery

Assuming stents were deployed in homogeneous, nonlinear hyper-elastic arteries model, all strut members have identical rectangle cross-section. Then structure of stent can be defined by several important geometrical parameters in the Table 2.

Table 2: Geometrical Parameter of Stents

Representatives	Geometrical parameters
D	The nominal diameter of the cylinder
N_c	The number of circumferential units
N_v	The number of vertical units
l	The length of the strut members
α	The angle between the struts with the line paralleling axial line
t	The cross-sectional side length of the strut members (square)

The length (l) of the strut members of the cells and the total length (H) of the cylinder can be derived from geometrical relations, here the thickness of the stent equals to the cross-sectional side length of the strut members.

There are some basic relationships in geometric parameters of rhombus(Figure 23). The sides have equal length, opposite sides are parallel. The diagonals p and q of a rhombus bisect each other at the right angle. Then, for the stent, the total length (H) of the cylinder,

$$H = N_v q \tag{3.1}$$

$$\tan\alpha = \frac{p}{q}$$

$2\pi D \approx N_c P$, When$N_c \gg N$, Polygons near circle cylinder model.

$$(2l)^2 = p^2 + q^2$$

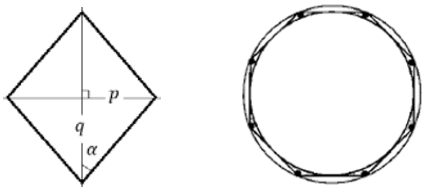

Figure 23: Stent structure includes arrangement of strut members

The length (l) of the strut members of the cells and the total length (H) of the cylinder can be derived from geometrical relations. The thickness of the stent equals to the cross-sectional side length of the strut members.

$$l = \frac{\pi D}{2N_c \sin \alpha} \tag{3.1}$$

$$H = 2N_v l \cos \alpha \tag{3.2}$$

In this model, for limited N_c, the diameter of the whole stent would be the dominator design parameter. For N_v, the length H has the exact relationship with the polygon;

According to the thin-wall cylinder theory(Figure 24), the longitudinal/axial stress (σ_z), circumferential stress (σ_c), radial stress (σ_r), and shear stress (τ) can be defined considering the axial load, pressure load on circumstantial and radial directions, and torque, respectively.

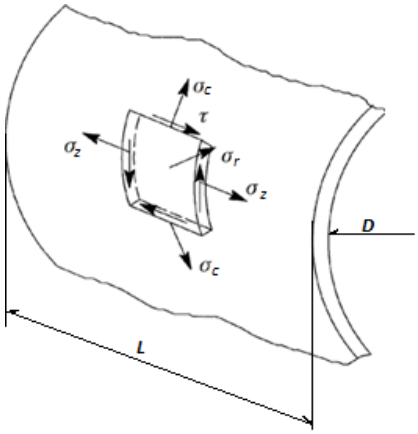

Figure 24: Stent theoretical modeling under external pressure and uniform axial and radial load

Then, the relative strains - axial strain (ε_z), circumferential strain (ε_c) and shear strain (γ_{cz}) can be represented as:

$$\varepsilon_z = \frac{H_f - H}{H}$$

$$\varepsilon_c = \frac{D_f - D}{D}$$

$$\gamma_{cz} = \frac{D\varphi}{2H}$$

Where φ is the relative axial angular rotation of cross-sections corresponding to the edges of the cylinder, H_f and D_f are the total length and diameter of the deformed cylinder, respectively. The mechanical properties of the stent can be calculated relating to the exact structure. Using parameters, the diameter of the cylinder$D$, the number of circumferential units N_c, the angle α, the thickness of the stent (or the cross-section size of strut) t and the Young's modulus of material E_m.

For small deformations (after balloon expansion), the mechanical properties of cylinder structure can be calculated with assumptions that the struts work as fixed-guided beams and adopting some beam approaches. This structure can be envisaged to deform when loaded by flexing and stretching of struts and by hinging at the struts junctions. Then, some mathematical models based on one or two of these mechanisms for some specific geometry are formulated. Using simple mechanics to calculate the deflections in each beam the strains induced in an individual unit and hence the whole network can be determined; enabling expressions for the moduli is written for the condition of uniaxial loading.

3.3.2 Stretching Force as a Uniaxial Loading on Rhombus Unit

The extension of the strut with length l due to the axial force acting along the stent is considered. The model assumes that the stent is only able to deform by stretching along its axes

with no change in angle.

Consider a cell subjected to a tensile loadσ_z in the axial direction (Figure 25). The load acting on the unit cell due to the applied stress $w = tlcos\alpha \cdot \sigma_z$ and the component P of w acting along the cell wall of length l is

$$P = t\sigma_z lsin\alpha \cdot cos\alpha \tag{3.3}$$

The strut is treated as a uniform beam of thickness t, wideness b, length of the beam (strut) l, K_s represents the stiffness of stent when stretching force enforced on the axial direction, E_m is the material Young's modulus. σ_z, ε_z are the stretching stress and strain along the axial direction, respectively.

The load acting on the unit strut due to the applied stress derives the effective Young's moduli:

$$\varepsilon_z = \frac{t\sigma_z cos\alpha \cdot sin\alpha}{K_s} \tag{3.4}$$

$$E_z = \frac{bE_m}{l \cdot sin\alpha \cdot cos\alpha} \tag{3.5}$$

In the same way to get another direction effective Young's moduli: $E_c = E_z$

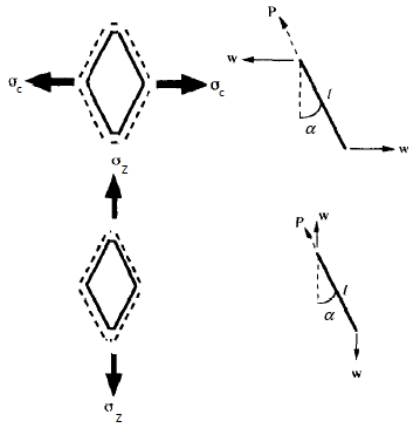

Figure 25: (Above). Struts deflection in c direction under uniaxial stretching loading; (Below). Struts deflection in z direction under uniaxial stretching loading.

3.3.3 Flexure Force as a Uniaxial Loading on Rhombus Unit

A strut of length deforming by flexing can be likened to a cantilever beam loaded at one end and fixed at the other. Using the geometric configuration and coordinate of stent, it is assumed that deformation occurred by flexing of the strut. Treating the struts as beams and using beam mechanics to derive the equations for the elastic properties of stent. The deflection of the guided end due to flexing is given by circumstantial and axial forces as following Figure 26 deformed shape of rhombus stent .vs. deformed bending struts:

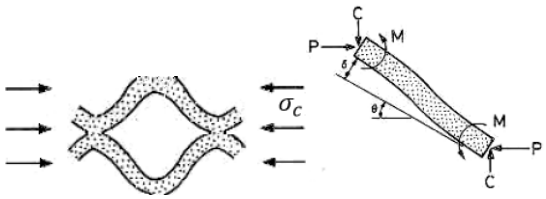

Figure 26: Struts deflection in circumstantial direction based on beam theory;

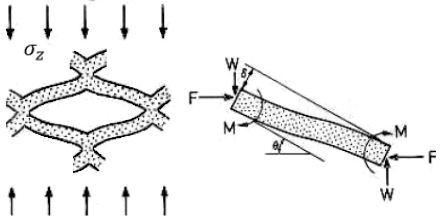

Figure 27: Struts deflection in axial direction based on beam theory

Assuming the strut is bended in a linear-elastic way, the moment bends the strut which is viewed as a strut of length l, widness$b$, thickness$t$, and Young's modulusE_m, σ_c is the flexure stress in the circumferential direction. In Figure.26, $\alpha = 90 - \theta$

$$M = \frac{Pl \sin\theta}{2}$$

$$P = \sigma_c tl \sin\theta$$

According to standard beam theory, the strut deflects by:

$$\delta = \frac{Pl^3 \sin\theta}{12E_m I} \tag{3.6}$$

For a beam of uniform thickness t, the second moment of inertia $I = \frac{tb^3}{12}$,

(If cross section is square, $I = \frac{t^4}{12}$),

$$\varepsilon_c = \frac{\delta \sin\theta}{l\cos\theta} = \frac{\sigma_c t(l\sin\theta)^3}{12E_m I\cos\theta} \tag{3.7}$$

$$\mathrm{E}_c = \frac{\sigma_c}{\varepsilon_c} = \frac{12E_m I\sin\alpha}{t(l\cos\alpha)^3} \tag{3.8}$$

When polygons near circle cylinder model, the equation will be near to the following value:

$$\mathrm{E}_c = \frac{8E_m sin\alpha}{(\cos\alpha)^3}\left(\frac{bN_c sin\alpha}{\pi D}\right)^3 \tag{3.9}$$

In Figure.27, the axial direction, the force$F = 0$, and $W = \sigma_z\, tlcos\,\theta$

$$M = \frac{Wl\cos\theta}{2}$$

Then, the strut deflects in axial direction by:

$$\delta = \frac{Wl^3\, cos\,\theta}{12E_m I} \tag{3.10}$$

$$\varepsilon_z = \frac{\delta\cos\theta}{l\sin\theta} = \frac{\sigma_z t(lcos\theta)^3}{12E_m I\sin\theta} \tag{3.11}$$

Effective Young's modulus in the axial direction derived as the ratio between the axial stress and the corresponding axial strain.

$$\mathrm{E}_z = \frac{\sigma_z}{\varepsilon_z} = \frac{12E_m Icos\alpha}{t(lsin\alpha)^3} \tag{3.12}$$

When polygons near circle cylinder model, the equation will be near to the following value:

$$\mathrm{E_z} = \frac{8E_m cos\alpha}{\pi^3}\left(\frac{bN_c}{D}\right)^3 \tag{3.13}$$

By summing the deflections in directions axial and circumferential, the two models stretching and flexure models could be combined to obtain a general expression. I.G. Masters and K.E. Evans once derived this general expression of honeycomb model [79]. Then the strain in axial direction caused by flexure and stretching could be accumulated and total strain would be obtained by summing equations (3.4) and (3.11), for example, the effective Young's modulus is available for the stent. However, the stretching part has less effect on the effective properties.

$$\mathrm{E_{ztf}} = \frac{b^3 E_m cos\alpha}{lsin\alpha[(lsin\alpha)^2 + (bcos\alpha)^2]} \tag{3.14}$$

$$\mathrm{E_{ctf}} = \frac{b^3 E_m \sin\alpha}{(l\cos\alpha)^3 + b^2 lcos\alpha(\sin\alpha)^2} \tag{3.15}$$

When considering the hinge on the connection part of each unit, the length of the connection is set as *h*, then the effective Young's modulus would be as the follows based on the result of I.G. Masters and K.E. Evans' general expression of honeycomb model[79] :

$$\mathrm{E_{zm}} = \frac{E_m b^3 cos\alpha}{l^3\left(\frac{h}{l} + sin\alpha\right)(sin\alpha)^2} \tag{3.16}$$

$$\mathrm{E_{cm}} = \frac{E_m b^3\left(\frac{h}{l} + sin\alpha\right)}{(lcos\alpha)^3} \tag{3.17}$$

Then considering the factors that, the connection length of each unit, the combination of flexure and stretching condition, updated equations for the effective Young's modulus are derived as follows:

$$E_{ez} = \frac{E_m b^3 \cos\alpha}{l\left(\frac{h}{l}+\sin\alpha\right)\left[\left(l\sin\alpha\right)^2+(b\cos\alpha)^2\right]} \tag{3.18}$$

$$E_{ec} = \frac{E_m b^3\left(\frac{h}{l}+\sin\alpha\right)}{\left(l\cos\alpha\right)^3+b^2 l\cos\alpha\left(\sin\alpha\right)^2} \tag{3.19}$$

The stent expands the constriction of artery vessel. Then it should have the proper rigidity in radial direction to keep enough blood stream pass through without damaging the artery wall. While the stent should be flexible enough to fit various anatomical bends. In the design of stents, the rigidity and flexibility would be considered carefully. For stents based on expansion method, balloon-expandable stents and self-expandable stents are widely studied. Considering the expandable stents, the longitudinal flexibility, radial stiffness and circumstantial deformation are analyzed here to supply advices for designing the stent structure.

3.4 Results and Discussions

3.4.1 To Verify Theoretical Results by Numerical Models

In this study the struts flexure model was used to determine the Young's moduli of theoretical molecular structures, and compared the results with those obtained by finite element analysis(Figure 28, Figure 29). The simple flexure model was mainly studied to consistently estimate the values of E by considering the plaque formed in the artery. A similar analysis on the stretching force is introduced and verified as well.

By referring the basic stent model with 16-strut in cross-section has 8 rhombus shape units(Figure 29). Table 3. shows the available Express stent made by Boston Scientific with similar

structure except that the thickness is not identical to the width of strut(0.05mm). By comparison, the structure of stent studied in the paper has the cross section of square.

Table 3. Physical Parameters of Express Stent (Boston Scientific) and Reported Restenosis Rates

ITEM	Express Stent(Boston Scientific)
Metal/Artery area ratio	27.12%
Material	316LN Stainless steel
Length	15 mm
Outer diameter	3.0mm
Strut width	0.05mm
Strut thickness	0.15 mm
No. of units along circumferential	8
6-month restenosis rate	19% [FDA approval P0200009 Sept.11,2012]

Take the studied model as an example, sets of stents characterized by ranges of variation in the angle α, the length of strut l and the number of circumferential cells N_c are related to each other if the stent expended in the artery without considering the preloaded force caused by the bubble.

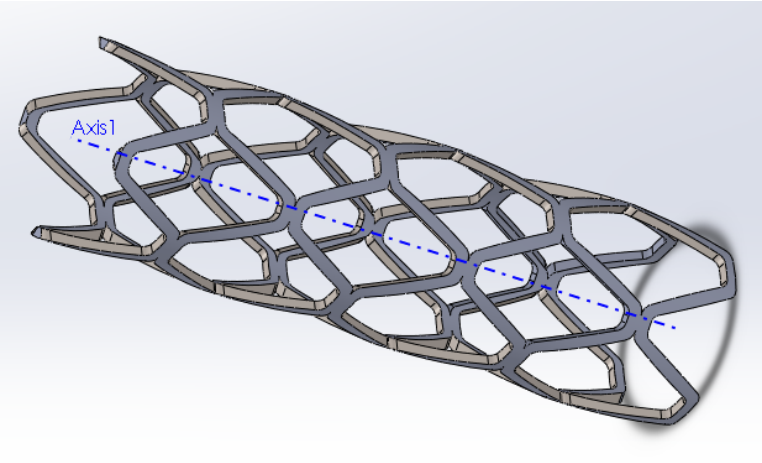

Figure 28: Structure of stents with 4 rhombus units – 8 struts

The angle between the struts and the length of strut, and the variable cross-sectional size of strut all impact the shear deformation of the beam members of stent, which should be considered. However, if the cross-sectional side length t of all cell members was chosen to obey

the restriction $t < 0.05l$, the shear deformation of the beam members of the cells could be neglected and here, set constant in these analyses of stent shown in the Figure 29.

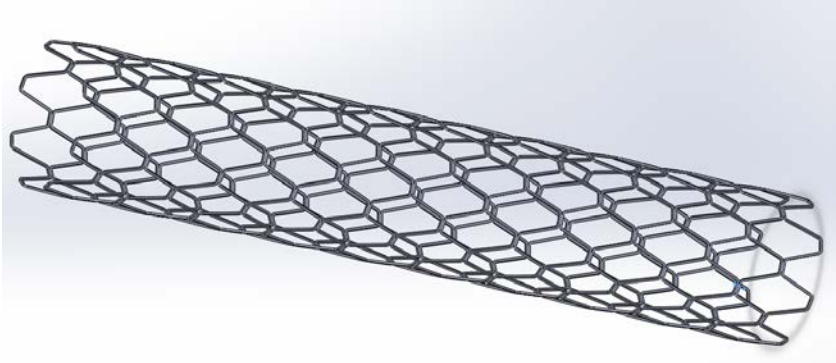

Figure 29: Structure of stents with 8 rhombus units – 16 struts

3.4.2 Material Models

The metallic stents are modeled as linear elastic-plastic materials. The composite metals differ in degrees of strength and flexibility. Specific materials and designs could be chosen to create greater thrombo-resistance. Some manufacturers choose cobalt chromium as a metal that is more radiopaque and durable than stainless steel.

Moreover, linear elastic material used here for modeling strut units. For each strut, it has unit elastic modulus and Poisson's ratio equals to 0.3.

Table 4. Materials Properties of Available Stents

Material Props	316L stainless steel
Young's modulus	190Gpa
Poisson ratio	0.3
Yield stress	207Mpa
Limit stress	515Mpa
Limit nominal strain	60%
Validated by	Auricchio et al.[2001] [85]

3.4.3 Result Comparison between Theoretical Model and Numerical Model

The numerical analyses were realized by using the MSC software NASTRAN finite element software package. Without the shear modulus study, axial forces are enforced on one end of model with another end constraint in axial direction. In order to verify the properties in the axial and circumferential direction, pressure is enforced to cause hoop deformation on this stent model. Another model is simulated for the bending case by a force loaded and guided at one end and fixed at the other one, like a cantilever beam. All enforced force is within the region ($\sigma_F = \frac{F}{A} << \sigma_y = 207Mpa$) which less than the value in order to ensure the analyses are done in the elastic region. The numerical models were created to compare their global mechanical properties with those predicted by equations (3.8)-(3.9) and (3.12)-(3.13). In verification models, the mesh size impacts the numerical results dramatically. Figure 31. Shows the results of different mesh size which will lead to different results. Refined mesh attributes to get real value than coarse mesh. See Figure 30 and Figure 31, the model with TETRA10, Angle =20°, Nc = 8, the refine mesh leads to convergent real value and the coarse mesh caused large error in the simulation.

Figure 31 shows the numerical results tend to a stable real value of structure properties of model with TETRA10, Angle =20°, Nc = 8, after mesh size is smaller than 0.02, when mesh size=0.0005, the result is quite identical to the one with mesh size=0.001. But in the following Figure 32, the graph indicates that less than 0.001mm mesh size will cause more time consuming, although the value had tended to the exact one but the consumed time is three times more than the previous setting. Therefore, in later analysis, the mesh size for such model would be set to 0.001.

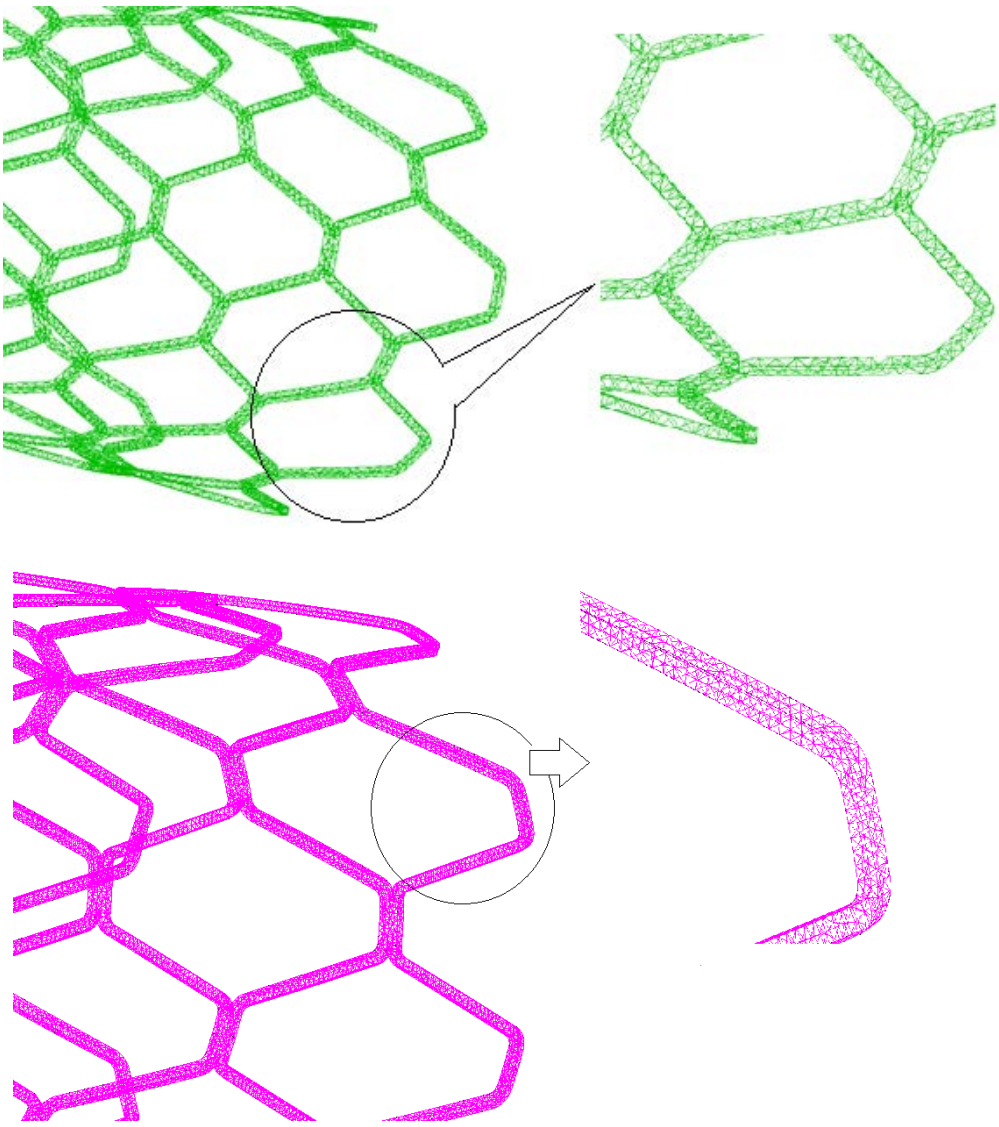

Figure 30: Comparison of different mesh size on FEA models:
Above: Edge length of element =0.001; Below: Edge length of element= 0.0005

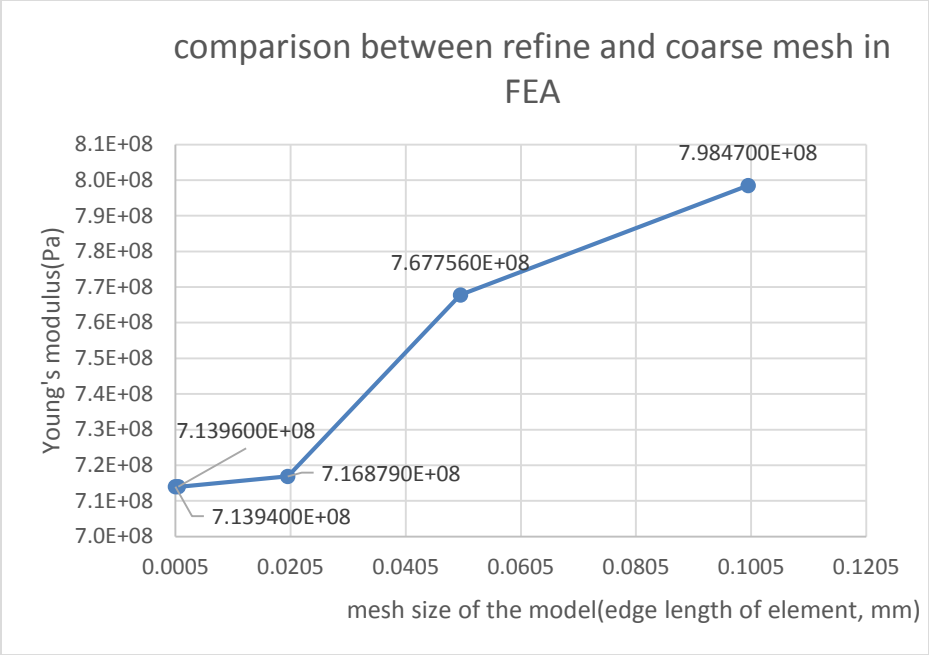

Figure 31: Comparison of different mesh size on FEA models: mesh from 0.1 to 0.001

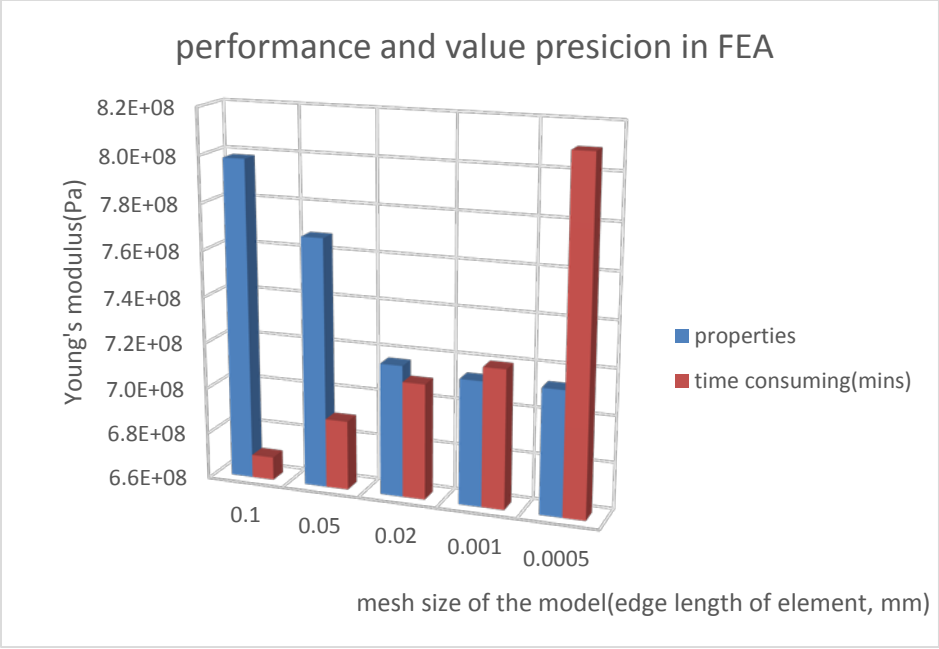

Figure 32: Comparison of consumed time for different mesh size on FEA models: Mesh from 0.1 to 0.0005

As the premise of the theoretical equation derived, the beam element simulates the structure and in basic unit structure testing, the theoretical value is near to the numerical value. The error is around 1%. Hopefully, the theoretical results should be near to the real value for the whole structure of stent, but for the rhombus structure, the sharp connection part can't be totally idealized in the modeling. Therefore, the length of the hinge which connected with each unit structure should be considered into the calculation equation(3.16)-(3.17). Moreover, the elastic modulus in the axial direction E_{ez} is determined by the value in the many conditions, mainly flexure condition, the stretching condition, etc. Although the axial part has relatively less effect on the structure, it also impacts the effective value of theoretical model. Therefore, the combination of these two conditions tends to near the real value(3.14)-(3.15). By varying the angle α, the length of strut l or the number of circumferential cells N_c are updated correspondingly. To analyze the resulting reaction forces on the ends and the changes in the total height H and the cylinder diameter D in FEA models help to verify the effective properties of this structure. Again, the elastic modulus in the circumferential direction E_{ec} and the radial compliance C were determined by radially deforming the cylinder diameter with an expanding cylindrical surface, coaxial with the stents. For the model has Mesh =0.001, Angle =20°, Nc = 8, axial loading results for axial Young's modulus:

Table 5. Comparison of Different Derived Equations for Properties in Axial Direction

Equations	FEA (tetra)	(3.12)	(3.13)	(3.14)	(3.15)	(3.18)
E_{ez}	2.314e+8	3.36e+8	1.089e+8	3.315e+8	1.9817e+8	2.2773e+8

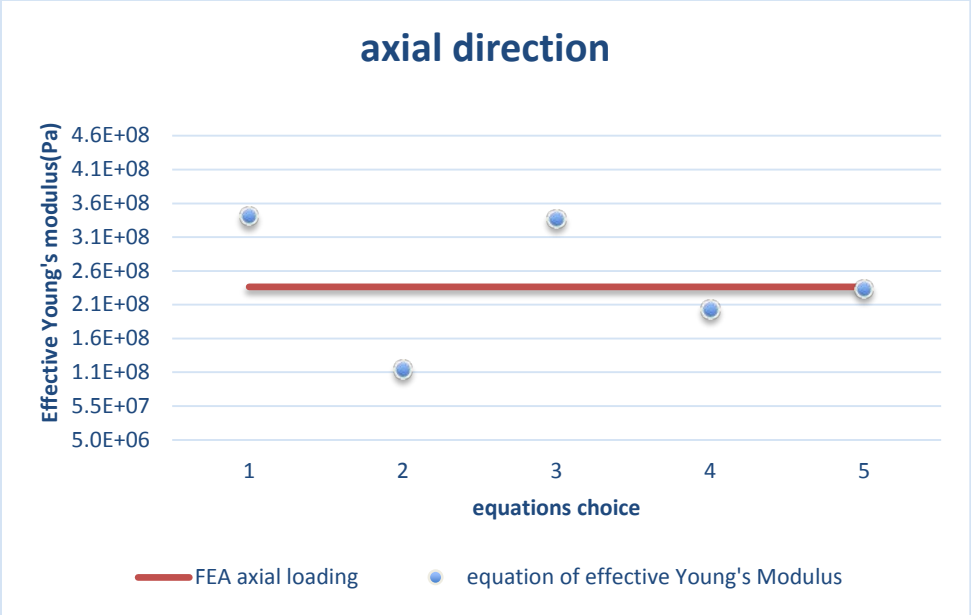

Figure 33: Comparison of derived equations for properties in axial direction with FEA results with axial loading; equation choice: 1-(3.12);2-(3.13);3-(3.14);4-(3.15);5-(3.18).

Blue points in FEA axial loading represent the results of effective Young's modulus based on different evaluation equations in axial direction. The results verify some important factors in the calculation of effective properties are necessary to be considered. Red line for FEA lists the FEA value which is near to the real value of the model. The numerical models follow the expected theoretical behavior with perfect error around 1.58%.

In the circumferential direction, the loading enforce on the stent is illustrated in the Figure34.

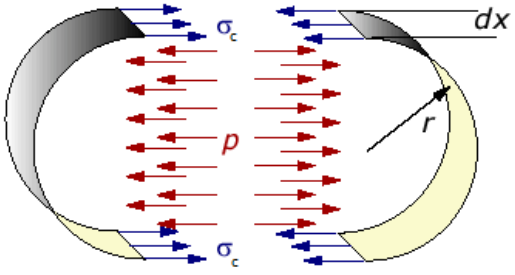

Figure 34: A slice of analysis model with internal pressure on the surface of stent[86]

The compared theoretical results and numerical results are shown in the Table 5 and Figure35. There are a large difference over 30% between theoretical results and numerical ones, the main consideration is related to the modeling approach. The modeling approach is to create a tube firstly, and then cut the hole on the tube. The assumed angle in the model is not precise to the actual angle(in this case, Angle =20°). In the circumferential Young's module equations, the item $(cos\alpha)^3$ makes the equation sensitive to the modeling approach. Therefore, all of the equation for the circumference properties did not match with the numerical results.

Table 6. Comparison of Different Derived Equations for Properties in Circumferential Direction

Equations	FEA(tetra)	(3.8)	(3.9)	(3.13)	(3.16)	(3.19)
E_{cz}	4.9357e+7	6.875e+6	2.2296e+6	6.8733e+6	1.1655e+7	1.165e+7

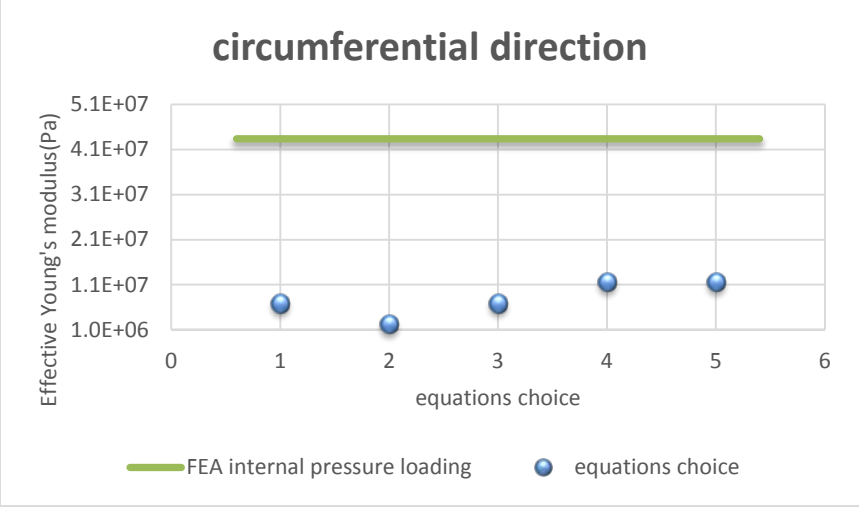

Figure 35: Comparison of derived equations for properties in axial direction with FEA results with axial loading; equation choice: 1-(3.8);2-(3.9);3-(3.13);4-(3.14);5-(3.19).

Again, if underling the bending condition, shown in the Figure 36, the FEA result has a little bit higher effective Young's modulus(green points) than the value of effective Young's modulus in axial direction(red line). When considering the possible situation of stent in the artery, the plaque generated at one point of the artery wall caused the bending effect on the stent.

Therefore, the properties(Young's modulus) in the axial direction is more straightforward to illustrate the properties of stent than other parameters.

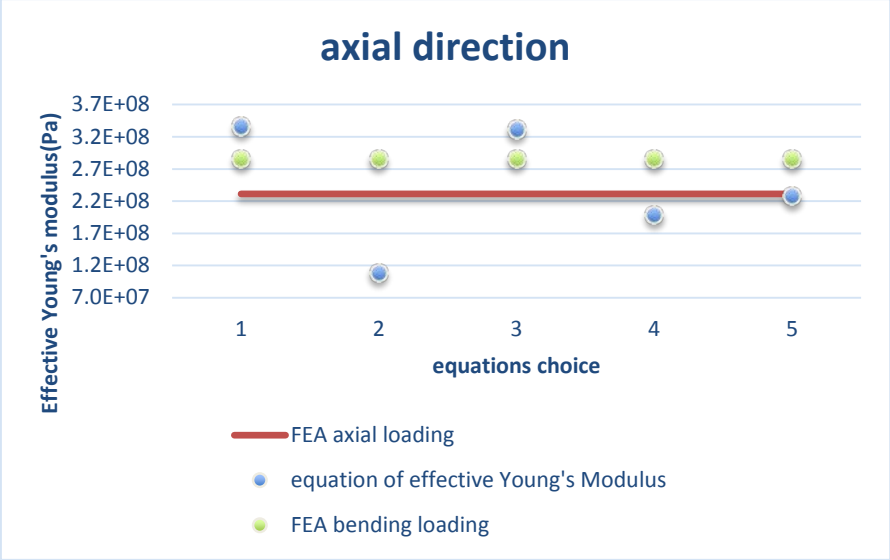

Figure 36: Comparison FEA results with bending loading and that with uni-axial loading

3.5 Conclusion

The diagrams of the effective Young's moduli E_z and E_c in the previous conditions obtained for model in FE linear analyses, are represented in previous figures. Compared numerical analysis results with the respective values obtained from the corresponding series of analytical equations, those differences between the values of the various mechanical properties between the numerical analyses and from the analytical models, several conclusions are shown here.

1. The length of the connection h is quite sensitive to the practical model error, especially for rhombus/diamond structure, round introduces geometric error and impacts the theoretical equation of effective properties. This portion includes the connectors linking struts together at nodes and restrictions on the slots cut into the tube from manufacturing limitations;

2. In circumferential direction, the evaluation can't get the ideal verification even if the connection part and the stretching condition effect are considered.

3. Using polygon instead of circle in cylinder cross-section causes more larger error. Then, when the number of circumferential units didn't reach a large value, the theoretical evaluation is unreliable, the error is over 30%. The approach is not a way to estimate the properties of the circumferential structure.

4. The Young's modulus in axial direction is reliable (error less than 2%) and reflects the property of the bending condition of the whole stent.

The mechanical properties of stent based on the rhombus structure were calculated by means of analytical and numerical approaches, respectively. Numerical models were used to analyze the response of these structures under various and complex loading condition. Then, these theoretical equations of the effective Young's module can be used to predict the deformation configuration of stent under specific loading condition according to different input material parameters. It is a way to simplify the stent structure and modify the geometric parameters to satisfy the requirement of stent functionality before modeling the complex structure in the numerical simulation.

The study verifiecd the influence of the geometric parameters defining the stent and predict the effective properties of the structures designed which contributes to the design the structure with requirement.

CHAPTER 4

COMPUTATIONAL APPROACH TO STUDY NON-LINEAR DEFORMATION OF STENT MECHANICS

4.1 Objective

The previous chapter3 linear analysis gives an evaluated properties of the structure (Young's modulus in two directions). Actually, real situation are too complicated and lead to the simulations with contact points, nonlinear geometry, large deformation, sample buckling, stent bending, and stress-strain nonlinearity. The main purpose of chapter 4 is to employ FEM for the evaluation of the impact of expending stent. Under internal pressure, the characteristics nonlinear behavior of the stent, the results show the plastic location on the stent and the stress locates in the elastic limit, the stent will recover its initial configuration after removal of the compressive load. The maximum equivalent stress is shown to occur at the 4.5 millimeter expansion diameter.

4.2 Introduction of Expandable Stents

Stents with tubular cellular structures develop in numerous cell shapes and sizes and in balloon-expandable and self-expanding varieties. The above-mentioned chapter provide a way for the identification and characterization of the stent behavior in linear analysis. However, there is still a need for more advanced and efficient models that consider the highly nonlinear behavior of the stent in the artery and further research on the complexity of their contact interaction. Characteristics, such as fore shortening, elastic recoil and dog-boning of balloon-expandable stents have been studied in finite element analysis with modeling and experimental verification of expansion mechanism of stent[87]. Here, stent expansion can be analyzed assuming struts within a stent expand at a constant rate via a plastic hinge mechanism. For each single hinge-strut unit,

the beam theory continuously contributes to the understanding of the complex and nonlinear inflation of expandable stent, and the finite element model could estimate and reproduce the characteristics crimp and inflation mechanism.

Most finite element models simulate pressure applied to the inner surface of the stent and are validated through in vitro expansion of stents. Unit structure analysis sometimes reflects the deformation of the whole stents and the entire stent simulations predict expansion deflection and stress/strain as well. Again, stent geometry optimization studies have shown the benefits of decreased stress concentration and elongate fatigue period. As the potential small cracks or contaminants contained in most materials, lead to the stress concentrate and therefore, the real fracture stress(limit stress) is lower than the theoretical value. Amount of stent designs and complicated computational modeling techniques arouse more attention to comparative methodologies for various stent designs. Among them, the fundamental understanding of the stent unit structure expansion mechanisms and following structure optimization will get optimal stent design.

The 3-4.5mm inflation of the cylindrical stent in arteries are subjected to significant mechanical loads and appears nonlinear characteristics. Geometric nonlinearities and material nonlinearities are considered in the analysis for stents. The three-dimensional finite element model is used to simulate the stent inflation characteristics. An empty and collapsed balloon on a guide wire, known as a balloon catheter, is passed into the narrowed locations and then inflated to a fixed size using water pressures some 75 to 500 times normal blood pressure[88]. Most normal healthy arteries yield an average hoop stress of approximately 100 KPa. This value again appears to hold over a wide range of conditions in many animal species[30]. By simulating the structure, the

maximum stress could be evaluated as a result of stent inflation to an inside diameter of up to 4.5 millimeters.

4.3 Approach on Expansion Mechanisms of Expandable Stents in the Artery

The non-linear FE model is based on the stents in chapter 3. Features of stent need geometry corrections in terms of a plastic hinge at each connection joint. The potions include the connectors linking struts together at nodes and restrictions on the slots cut into the tube from manufacturing limitations. Stent expansion is analyzed assuming struts within a stent expand at a constant rate via a plastic hinge mechanism. Then the strut unit can be the analytical model and illustrated as the following Figure 37.

This model of expansion considers a bending stent strut as pairs of cantilevers loaded by a point force at the connection part, applied perpendicular to the initial cantilever position. During the expansion procedure, the sixteen struts in a circle grow along the sphere and viewed as bending struts[81]. The circumferentially connecting parts which deformed without bending. Then the stent expands δ_z in the axial direction and δ_c in the circumferential direction. Furthermore, the plastic hinge in the struts at the connection region, labelled on the joint, for the bending analysis, this part of struts represent radius of curvature r and the deformation of the length of strut l' in the plastic region.

The stent was originally positioned outside the artery and then translated in the axial direction such that the stent and artery midpoints along that direction coincided[81]. The pressure was then reduced to systole and subsequently to diastole. Then, the vessel was then inflated by applying a pressure of 225 mmHg(30 kPa). This pressure dilated the artery enough such that the 10% oversized stent could be “implanted.” As a reference, furthermore, the Law of Laplace

estimates the circumferential wall stress to an unstented artery with identical geometric dimensions as approximately 83 kPa at diastolic pressure[89]. The value serves as a general reference guideline for evaluation of the extremely high non-physiologic, stent also induced stress values placed on the artery wall.

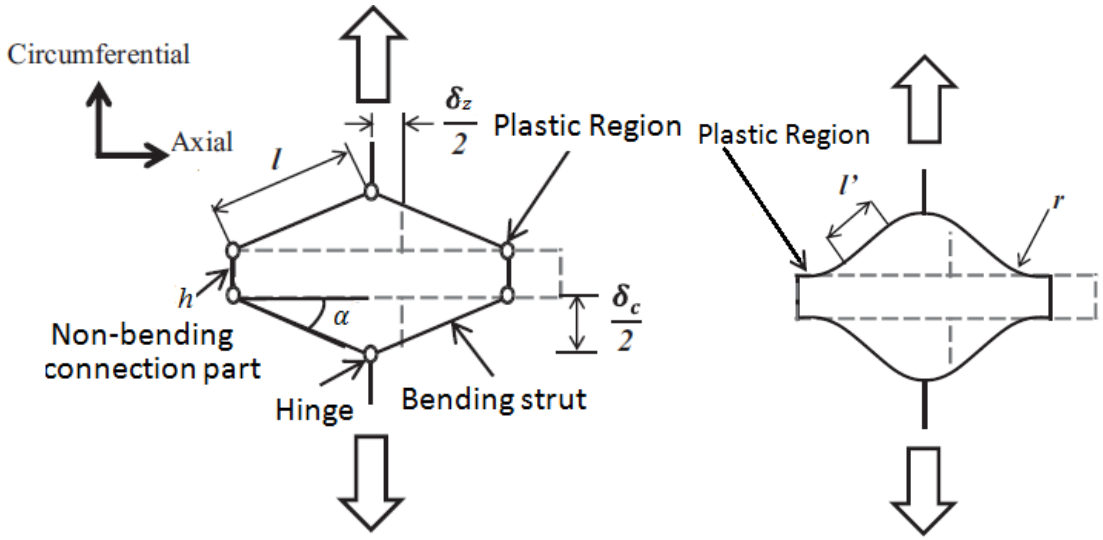

Figure 37: Nonlinear analysis(inflating stent with balloon) for stent with rhombus structure considering the connection part of model. (a) idealized analytical model in non-linear analyses. (b) part curvature of plasticity region due to the expansion forces[81].

The analysis of the stent inflation involves a model with large deformations and large strains. Therefore, nonlinear material properties need to be considered to accurately describe the deformation process. The Lagrangian or material method describes that the material associated with an element remains associated with the element throughout the analysis, and material cannot flow across element boundaries. In the alternative Eulerian or spatial description, elements are fixed in space as the material flows through them. Eulerian methods are used commonly in fluid mechanics simulations. Nastran, Marc or Abaqus are all based on Lagrangian or material description. The numerical method uses Gaussian quadrature to integrate various quantities over

the volume of each element. Again, the material response at each integration point in each element, here, full integration is chosen.

During the nonlinear analysis, the total Lagrangian and the updated Lagrangian method are considered with respect to the un-deformed configuration. In this case, the inflation of the stent is modeled using an elastic-plastic material model, inelastic strains, which cause large deformations.

Solution of nonlinear equations, ${}^{t+\Delta t}R$ is externally applied loads, ${}^{t+\Delta t}F$ is nodal point forces corresponding to internal element stresses [90].

$$ {}^{t+\Delta t}R - {}^{t+\Delta t}F = 0 \tag{4.1} $$

In the iteration, $i = 1,2,3, \ldots$ ${}^{t}_{0}k$ means the stiffness matrix of the structure at initial state, Δu is the displacement.

$$ {}^{t}_{0}k \cdot \Delta u = {}^{t+\Delta t}R - {}^{t+\Delta t}_{0}F^{(i+1)} \tag{4.2} $$

At convergence, we satisfy the compatibility, stress-strain law and equilibrium of nodal point and local force and get the following equilibrium equation.

$$ {}^{t+\Delta t}R = {}^{t+\Delta t}_{0}F $$

Therefore, the updated Lagrangian method is used in the frame due to the inelastic deformations, and the stress and strain calculations are based upon true (Cauchy) stress and true (logarithmic) strain measures. As mentioned introducation part of this chapter, the equivalent stress and equivalent strain are used as quantities to the analyzed values.

The analysis of a biomedical stent with a 3.0 mm nominal inside diameter design is performed for stent with rhombus structure unit by using MSC.NASTRAN nonlinear finite element analysis(implicit solution) (MSC. Software. Nastran, CA, USA). Geometric nonlinearities and material nonlinearities are considered in the analysis for stents. The three-dimensional finite element model is used to simulate the stent inflation characteristics. The aim of

the analysis is to evaluate the maximum stress as a result of stent inflation to an inside diameter more than 3.0 mm and crimped to an outside diameter in order to be placed into the cather. Concomitantly, computational methods were used to quantify the relations of mechanical loads and equivalent stress when stents place on the artery.

4.4 Results and Discussions

The numerical analyses were carried out using the MSC software NASTRAN finite element software package implicit solver SOL 400. The rhombus structure designs are reduced to half of their original size using one planes of transverse symmetry. Meshing is done with quadratic 10-noded tetrahedral elements(TETRA10). Approximate global sizes and chose mesh size=0.001 with five or six elements across the strut width. The material of stents is 316L stainless steel. Boundary conditions are applied to its ends and cut faces. One end fixed all axial displacement and the line along the total length of stent constrains displacement in transverse direction. The other end is free.

Mesh parameter of model and material properties are listed in the following Table 6.

Table 7. Model Properties and Mesh Properties

Edge length of element	Element Type	Number of elements	Number of nodes
0.001	TETRA10	35777	100113
Geometrical parameters	Angle =20°	Nc = 8	
316L stainless steel			
Young's modulus	190Gpa		
Poisson ratio	0.3		
Yield stress	207Mpa		
Limit stress	515Mpa		
Limit nominal strain	60%		
Material properties	Validated by	Auricchio [85]	

Subsequent to implant into the artery, assuming the stent is inflated to a maximum inside diameter by enforcing pressure 83 kPa and attained to the diameter of 4.5mm. Typically, inflation of the stent may be performed using direct pressure applied to inside diameter of the stent or manually expanding the stent through prescribed boundary conditions. Then referencing from the available literatures to enforce the precise pressures to expand the stent, the maximum stress in stent and deformed diameter are available to predict the structure configurations. Alternatively, inflation of the stent can also be performed by pressurization of an elastomeric balloon material inserted inside the tube. Following the balloon inflated, the stent diameter expands with each struts open. The expandable stage(green configuration) the stent is released and allowed to spring back to a 'free' state(blue configuration) as shown in top view Figures 38 and Figure 39. Equivalent stress shown on the contour of model is around 498MPa under more than 50% expanding (from 3.0mm to 4.5mm).

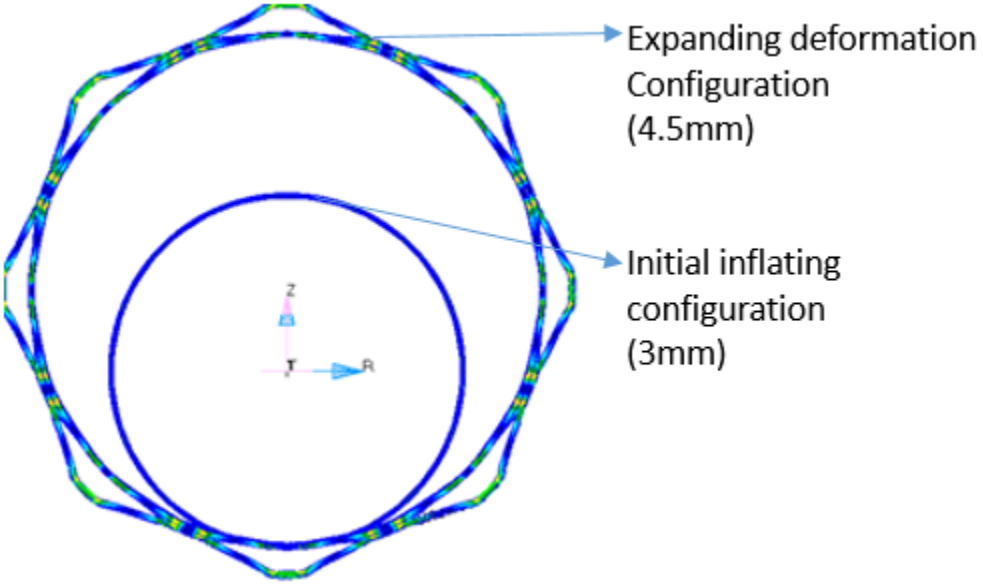

Figure 38: Initial stent inflating configuration(3.0mm) to inflated configuration(4.5mm)

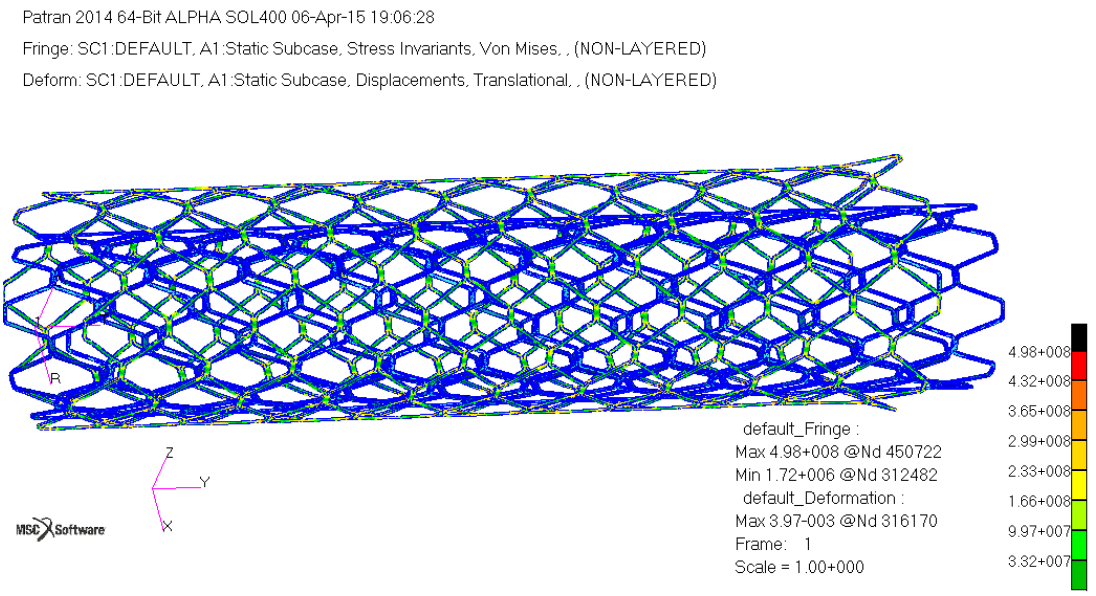

Figure 39: Initial stent inflating configuration(blue) to inflated configuration(green).

In the following figure 40, the contour of expanding configuration illustrated the maximum equivalent stress value of the structure, is around 498MPa. The plastic region(yellow and green color shown) right locates near the hinge joint part, which is discussed in the analytical approach.

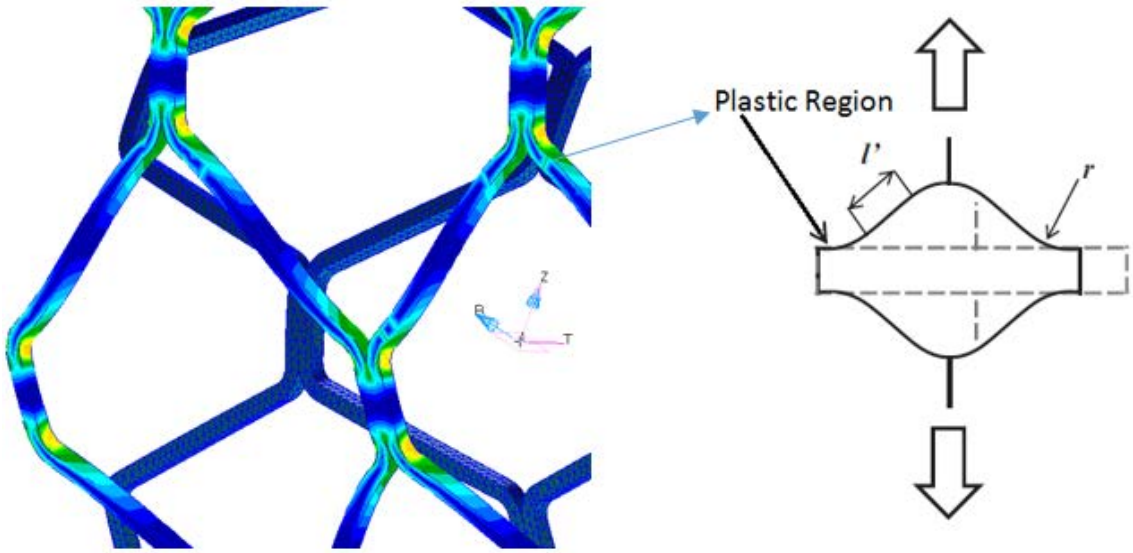

Figure 40: Stent inflating configuration, the maximum equivalent stress(yellow/red color location) occurs in the plastic region which consistent with analytical model

According to relative clinic report, the artery is subject to a high degree of mechanical force and deformation, which can increase the potential for complications related to permanent metal stents. These complications include stent fracture, persistent inflammation and in-stent restenosis[91].

During stent implanted in the artery, assuming the finite element stent model is compressed by using direct pressure applied to outside diameter of the stent or manually compressed the stent through prescribed boundary conditions. Subsequent to the compressed stage(green configuration) the stent is released and allowed to spring back to a ‘free’ state(blue configuration) as shown in Figures 41. Equivalent stress shown on the contour of model is around 407MPa under 30% compressed pressure(from 3.0mm to 2.1mm).

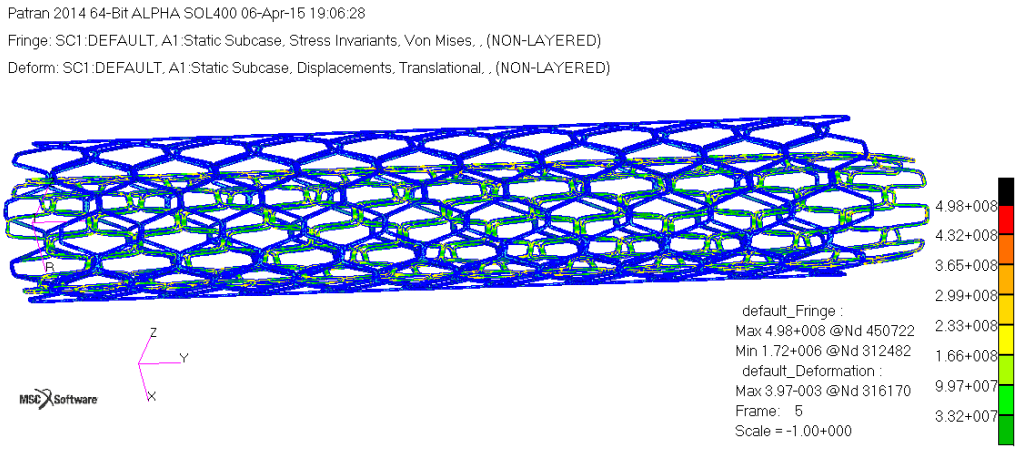

Figure 41: Initial stent inflating configuration(blue) to compressed configuration(green).

The descripted situation can be explained as the compression case in following Figure 42, which shows possible mechanical force and deformed configurations in the artery.

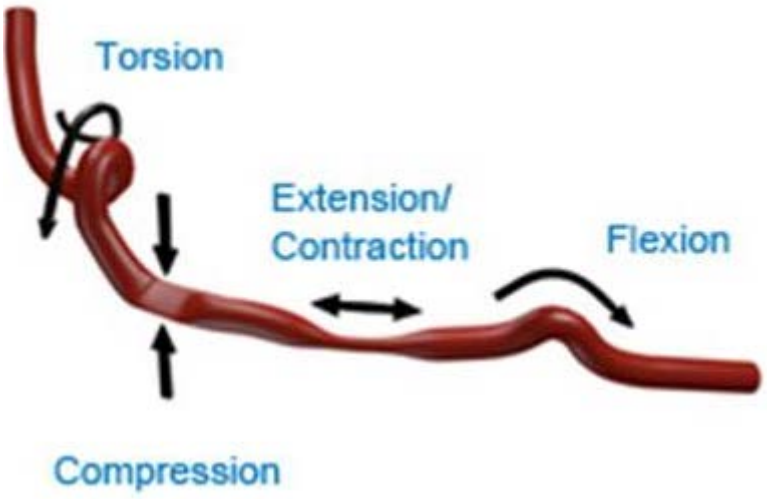

Figure 42: Mechanical force and deformed configurations in the artery [91]

4.5 Conclusion

In nonlinear analysis, the stress-strain data and ultimate strength are given using the engineering stress-strain measure. Therefore, the equivalent stress and equivalent strain are the important quantities to the analysis values in order to relate true stress and true strain measures to their respective engineering stresses and strains under multi-axis stress state.

Prior to the inflation simulation, the compression portion of the analysis was completed to determine the residual stresses induced in the stent when crimped, the stent was compressed from the manufactured diameter of 0.071 inches to 0.038 inches(1.8103 millimeters to 0.9652 millimeters). With the external pressure(model) or rigid body cylindrical cather surface(practical application), compression of the stent causes uniform radial deformation. So contacts between the cather and the stent, rigid body surfaces and self contact between struts are considered to be a future topic in the research.

It is noticed that the dominant change of loading appears to cause an increase tensile load in connection part. The stress is primarily caused and determined in terms of bending as the struts open and straighten out when stent is inflated. The maximum equivalent stress is shown to occur

at the 4.5 millimeter expansion diameter. Approximate equivalent engineering stress values calculated using equation (4.3), where ε_t= true strain and ε_e = engineering strain

$$\varepsilon_e = \exp(\varepsilon_t) - 1 \tag{4.3}$$

The true-stress value are typically larger than the respective engineering stress measure, which is commonly used with material test data. This must be considered when comparison of maximum stress results reported herein are to be made with engineering test data. Generally, the experimental data from a uniaxial tension test is expressed in terms of true stress vs. true strain, not engineering stress or strain. However, it is very difficult to relate the true stress measure to the respective engineering stress when a structure is subject to a three dimensional stress state as is the case for the stent inflation. In order to compare the results reported herein with material test, the true stress quantities can be converted to an approximate engineering stress. See Figure 43. The engineering stress-strain curve and using the estimated engineering strain value to estimate stress. Compared with the available stress-strain relationship graph(Figure 43) of AISI 316L stainless steel under monotonic load[92], the stress-strain relationship is shown in the Figure 44.

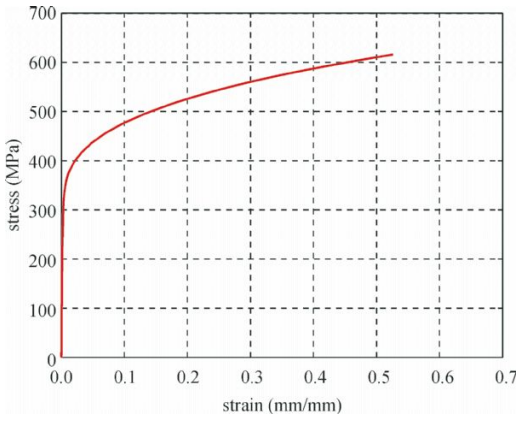

Figure 43: Stress-strain relationship of AISI 316L stainless steel under monotonic load[92]

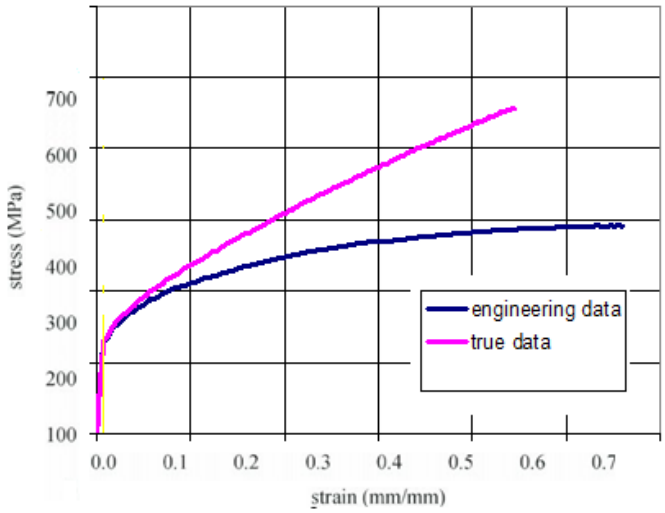

Figure 44: Stress-strain relationship of 316L stainless steel

The maximum stress values were found to occur in localized regions of the stent. These regions were generally found along the inner radii of each of the 'corner' links connecting each of the longitudinal struts. Stress values throughout the whole stent were typically much lower. The peak engineering stress values(498MPa) were found to be less than the material ultimate strength (limit stress 515Mpa), indicating a safe stent design throughout expansion range.

As shown in the graph, the stress in each of the radius sections exceeded the elastic material limit (207MPa), after removing compression loading, plastic (permanent) deformation was caused. If stress not exceeded the elastic limit, the stent will recover its initial configuration after compressive load disappeared.

CHAPTER 5

FUTURE WORK AND CONCLUSION

5.1 Conclusion Summary of Research Analysis

The mechanical properties of stent based on the rhombus structure were determined by means of analytical and numerical approaches. Numerical models were used to analyze the response of these structures under various and complex loading condition. The study identified the influence of the geometric parameters defining the stent on the phenomenon and predict that the adoption of structures appropriately designed can contribute to requirement functionalities of stents.

A successful analysis was completed for the inflation simulation of expansion of the stent with 84kPa. The maximum stress in the stent was found to occur in very localized regions at the small radii on the inside of the 'connector' of the stent longitudinal members. The maximum stress is primarily a result of in-plane bending or opening of the struts during stent inflation. The peak values diminished significantly away from the small radii and along the stent struts. The maximum expansion stress was found to occur at the 4.5 millimeter diameter.

Despite the implantation of vascular stent brings tremendous success, these medical devices also lead to some accumulated pathobiologic side-effects, such as excessive neointimal hyperplasia can result in the formation of a new blockage (restenosis). Relative researches based on clinical data conclude that stent design is a key factor in the development of restenosis. In addition, computational studies indicate that the biomechanical environment is strongly dependent on the geometrical configuration of the stent, and possibly involved in the development of restenosis.

Amount of stent designs and complicated of computational modeling techniques excites the researches for comparative methodologies for various stent geometry design. A fundamental understanding of the mechanics on the unit shape involving compress/inflate mechanisms and their modeling analysis definitely attribute to optimize stent designs. Combined clinical performance reports with FEA software to simulate the real physical situation, using refined numerical studies more complicated situations, such as stent-artery, stent-flow interactions will be the purpose in our future tasks.

The computational model employed to quantitatively characterize the hemodynamic conditions under simulated blood flow conditions in a an idealized model of artery. It will progress the potential application of computational blood flow simulations to stent implantation.

5.2 Future Work

The next step of this study will be to analyze stent mechanical behavior under artery and blood flow effect. This part allow us to develop future models that will easily match suitable stent configuration with the type of the patient diseases.

5.2.1 Objective

The major topic addressed in this chapter is to develop a computational fluid model(non-Newtonian) effects on the steady flow through an arterial segment using the well-developed blood constitutive equation. Non-Newtonian flow computations is carried out to examine the modeling effects in terms of the wall pressure and wall shear stress. It leads to further integration of the construction of models , solution of the governing equations and extraction of relevant information for intractable blood flow in an ideal artery. This part allow us to develop future models that will

easily match suitable stent configuration with the type of the patient diseases. The models will be applicable to personalized and improved patient care that will save many lives annually.

5.2.2 Introduction of Blood Flow in an Artery System

The arteries transporting blood maintain overall homeostasis of the circulatory system. Under normal conditions, arteries adapt to changes in blood flow and blood pressure. However, under certain circumstances, the arteries are unable to respond to the imposed forces and the adaptive and healing processes fail. Therefore, accurate characterization of artery geometry and blood flow is vital to understand the pathogenesis of atherosclerosis.

In order to understand the normal and pathologic behavior of vascular system, detailed knowledge of blood flow and the response of blood vessels is required. Clinically relevant plaque deposits are most common in areas of complex flow in the coronary, carotid, abdominal, and femoral arteries[93]. Three dimensional computer reconstructions based on medical imaging are now ubiquitous, some manufacturers obtain accurate stent geometry by segmenting nano/micro-CT images, and then transform micro-CT data and reconstruct them in 3D model(Mimics Innovation Suite). Some automated re-mesh technology is becoming instrumental in providing all necessary dimensions of the 3D structure to create approximate parametric models. The complex circumstance of the artery is hard to be comprehensively quantified by characterized parameters. However, understanding the features of healthy artery, and the rules of the blood flowing the vessel wall is primary to the future interactive analysis with implanted stent. Idealized vascular models and analyses combining accurate rheological models of blood and constitutive relations and mass transport properties for blood vessels prevail in current research. The extracted physical data from

the cross-sectional image of blood vessel helps simulate and predict the interaction among stent, blood and artery wall.

Generally, detailed experimental investigations into the mechanics of blood flow in the vascular system contributes to the understanding of vascular disease and long-term consequences of surgical repair. However, the complete field variations of variables(pressure, velocity and viscous stress) are infeasible to obtain, performing the experiments and extracting quantitative flow data is often a time consuming and expensive process; it is impractical to use working fluids with the same complex rheological characteristics as blood, or models with the same mechanical and transport properties as blood vessels; Moreover, the quantitative information extracted from the experimental flow studies is usually limited to a small number of velocity profiles or pressure measurements. Therefore, numerical analyses is widely performed whereby arteries have been approximated as branched channels to understand vascular hemodynamics [94, 95].

5.2.3 Preliminary Data of Study

Study introduction: As preliminary results we have obtained IVUS images from UTSouthwestern hospital for patient with the following conditions:

73 years old male

Prior smoker. Quit in 1991. Had been a smoker since age 13 smoking 3 packs per day at his highest use; family history of atherosclerosis and chest pain.

Two vessel coronary artery disease, patent (i.e. open) left internal mammary artery to mid-left anterior descending artery and patent right coronary stents. Successful percutaneous intervention of saphenous vein graft to obtuse marginal artery with overlapping drug-eluting stents x 4.

Figure 45 is a three-dimensional model developed from IVUS image using Dr. Horne's code, which simulates the blood flow in this section of artery.

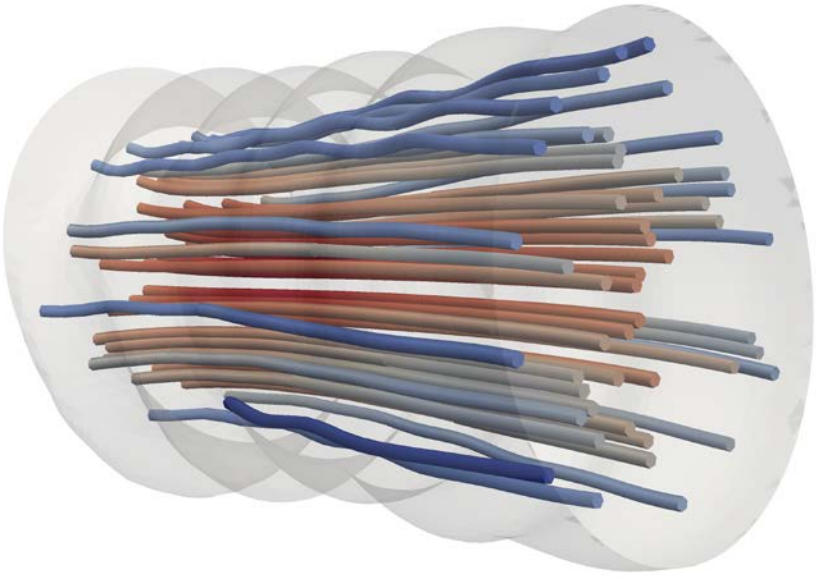

Figure 45: Three-dimensional model developed from IVUS image

5.2.4 Modeling of Case Blood Flow

The rheological behavior of blood can be quantified by non-Newtonian viscosity. Haldar illustrated that the rheology of blood and the fluid dynamical properties of blood flow are the key factors in the basic understanding, diagnosis, and treatment of many cardiovascular and arterial diseases[96]. In general, the computational blood flow model is three-dimensional and transient flow in deforming blood vessels. Newtonian fluid viscosity is always constant against the shear rate. By comparison, non-Newtonian fluid viscosity changes depending on the shear rate. Mir Golam Rabby demonstrates the relationship between blood viscosity and the shear rate for Newtonian and four different non-Newtonian models (Figure 46)[97]. Correspondingly, the Newtonian and other non-Newtonian models are illustrated in the following table 6.

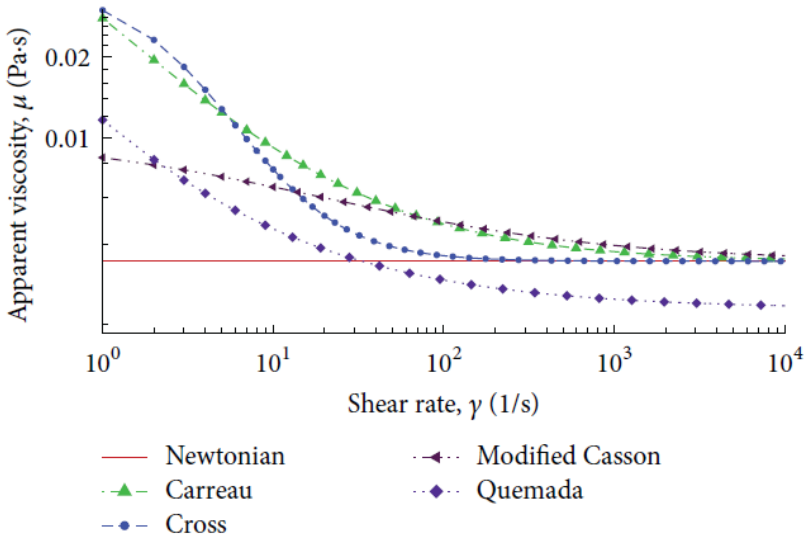

Figure 46: Relations between the shear rate and the apparent blood viscosity for the different models[97].

Table 8. Non-Newtonian Models with Given Molecular Viscosity of Blood[97]

Model	Effective viscosity
Newtonian	$\mu = 3.45 \times 10^{-3} Pa \cdot s$
Carreau	$\dot{\gamma}$ shear rate, μ_∞ constant viscosity (Newtonian fluid) $\mu(\lvert\dot{\gamma}\rvert) = \mu_\infty + (\mu_0 - \mu_\infty)[1 + (\lambda\dot{\gamma})^2]^{(n-1)/2}$ $\mu_0 = 0.056 Pa \cdot s$ viscosity at zero shear rate $\lambda = 3.131$ time constant, $n = 0.3568$ power law index
Cross	$\mu(\lvert\dot{\gamma}\rvert) = \mu_\infty + \frac{(\mu_0 - \mu_\infty)}{[1 + (\dot{\gamma}/\gamma_c)^n]}$ $\mu_0 = 0.0364 Pa \cdot s$ viscosity at very low shear rate $\gamma_c = 2.63 s^{-1}$ shear stress in the center line, $n = 1.45$
Modified Casson	$\mu(\lvert\dot{\gamma}\rvert) = \sqrt{\eta_c} + \frac{\sqrt{\tau_0}}{\sqrt{\lambda} + \sqrt{\dot{\gamma}}}$ $\eta_c = 3.45 \times 10^{-3}$, $\lambda = 3.131$ $\tau_0 = 2.1 \times 10^{-2} s^{-1}$, $n = 1.45$
Quemada	$\mu(\lvert\dot{\gamma}\rvert) = \mu_p(1 - \frac{1}{2}\frac{k_0 + k_\infty\sqrt{\lvert\dot{\gamma}\rvert/\gamma_c}}{1 + \sqrt{\lvert\dot{\gamma}\rvert/\gamma_c}}\phi)^{-2}$ $\mu_p = 1.2 \times 10^{-3}$, $\gamma_c = 1.88 s^{-1}$, $k_\infty = 2.07$, $k_0 = 4.33$, $\phi = 0.45$ for haematorcrit

(Mir Golam Rabby)

Generally, Reynolds number 300 is set for the incompressible, homogeneous and sinusoidal pulsatile flow. As an approximation, the artery wall is viewed as rigid body and blood is regarded as non-Newtonian fluids for the flow field computation. Features of Carreau flow shows a zero-shear plateau at low rates and a power-law region at high rates[97] :

$$\mu(|\dot{\gamma}|) = \mu_\infty + (\mu_0 - \mu_\infty)[1 + (\lambda\dot{\gamma})^2]^{(n-1)/2} \tag{5.1}$$

The model describes pseudoplastic flow with asymptotic viscosities at zero μ_0 (Newtonian) and infinite $\mu_\infty (n < 1$ non-Newtonian) shear rates and with no yield stress; λ is a constant with units of time , after $\lambda = 1/\dot{\gamma}$, non-Newtonian behavior is important; $n = 0.3568$ is power law index as a measure of the deviation of the fluid form Newtonian($n = 1$, Newtonnian fluid; $n > 1$, shear-thicking(dilatant fluid); $n < 1$, shear-thinning(pseudo-plastics)) (Ewoldt). The rate-of-deformation tensor $\overline{\overline{D}}$ and the shear rate $\dot{\gamma}$:

$$\overline{\overline{D}} = \frac{1}{2}\left(\frac{\partial u_j}{\partial x_i} + \frac{\partial u_i}{\partial x_j}\right) \tag{5.2}$$

$$\dot{\gamma} = \sqrt{2\overline{\overline{D}}:\overline{\overline{D}}} \tag{5.3}$$

The shear stress can be simply written in terms of a non-Newtonian viscosity $\mu(\dot{\gamma})$:

$$\tau = \mu(\dot{\gamma})D \tag{5.4}$$

In Carreau model, considering $u = 0, v = 0$, velocity won't change, $\frac{\partial u}{\partial x} = 0, \frac{\partial v}{\partial y} = 0, \frac{\partial w}{\partial z} = 0$.

Then, the momentum balance equation,

$$\rho\frac{\partial \vec{v}}{\partial t} + \rho(\vec{v}\cdot\nabla)\vec{v} = -\nabla P + \nabla\cdot\tau \tag{5.5}$$

X direction momentum,

$$\rho u\frac{\partial u}{\partial x} + \rho v\frac{\partial u}{\partial y} = -\frac{\partial P}{\partial x} + \frac{\partial}{\partial x}\left(\mu\frac{\partial u}{\partial x}\right) + \frac{\partial}{\partial y}\left(\mu\frac{\partial u}{\partial y}\right)$$

Y direction momentum,

$$\rho u\frac{\partial v}{\partial x} + \rho v\frac{\partial v}{\partial y} = -\frac{\partial P}{\partial y} + \frac{\partial}{\partial x}\left(\mu\frac{\partial v}{\partial x}\right) + \frac{\partial}{\partial y}\left(\mu\frac{\partial v}{\partial y}\right)$$

Z direction momentum,

$$\rho u \frac{\partial w}{\partial x} + \rho v \frac{\partial w}{\partial y} = -\frac{\partial P}{\partial z} + \frac{\partial}{\partial x}\left(\mu \frac{\partial w}{\partial x}\right) + \frac{\partial}{\partial y}\left(\mu \frac{\partial w}{\partial y}\right)$$

$\frac{\partial P}{\partial z} \neq 0$. Then, equation is simplified as:

$$\frac{\partial P}{\partial z} = \frac{\partial}{\partial x}\left(\mu \frac{\partial w}{\partial x}\right) + \frac{\partial}{\partial y}\left(\mu \frac{\partial w}{\partial y}\right)$$

$$\dot{\gamma} = \sqrt{\left(\frac{\partial w}{\partial x}\right)^2 + \left(\frac{\partial w}{\partial y}\right)^2} \tag{5.6}$$

5.2.5 Code Implementation

To compute the blood flow through two ends constricted artery, the solver is implemented to solve sequentially the momentum balance equation. The coupling between velocity and pressure drop is achieved through algorithm.

Analyze the continuity control volume as following Figure 47 in following discretized domain,

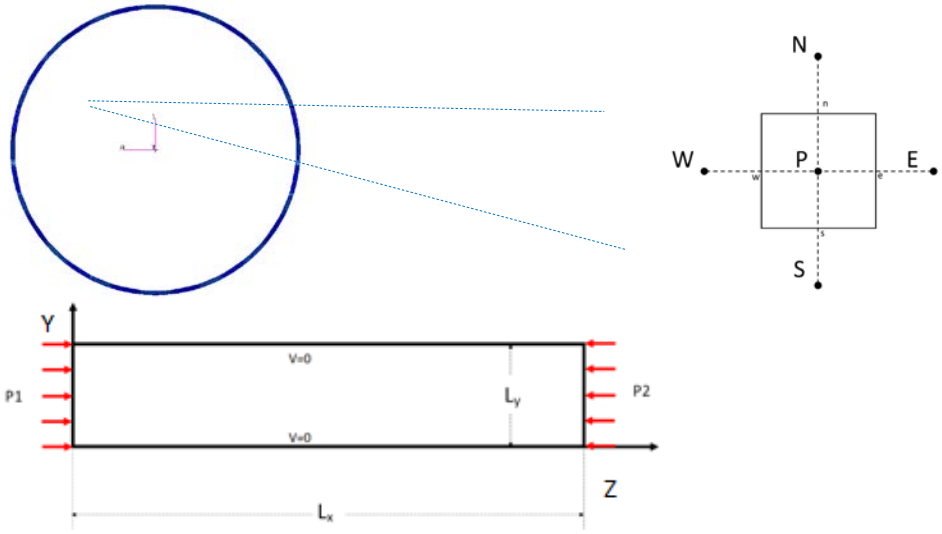

Figure 47: Segment of blood model field(cross-section of the artery) as the control volume of studied flow.

For the two-dimensional model, the viscosity at the control volume faces could be evaluated precisely by setting the grid points and draw control volume faces between neighboring points, See figure 48. Generally, the viscosity at n point can be interpolated as equation (5.7):

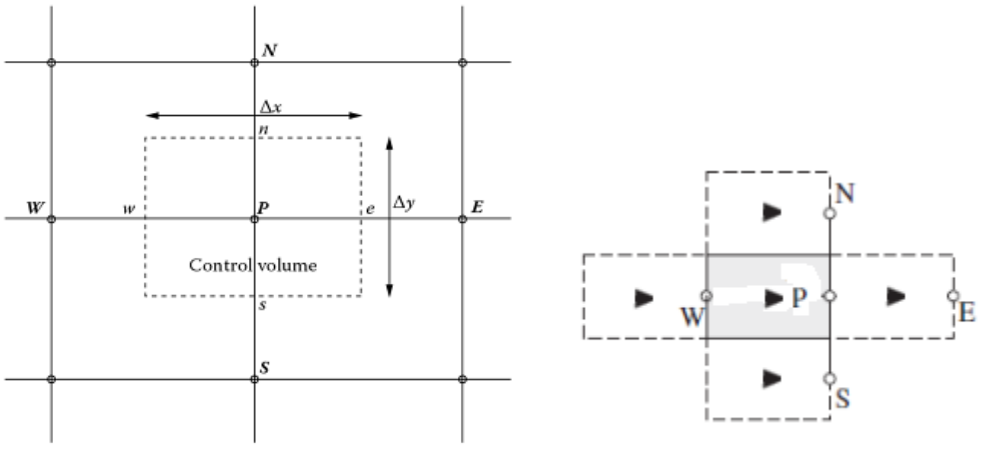

Figure 48: Finite volume cell with neighbor points in the control volume

$$\mu_n = \frac{2\mu_N \cdot \mu_P}{\mu_N + \mu_P} \tag{5.7}$$

Then the average velocity and the shear stress be derived in the control volume:

$$\overline{w} = \frac{\int_{cv} w dA}{\int_{cv} dA} \qquad F_{shear} = \oint \mu \frac{dw}{d\hat{n}}\, dl \qquad \hat{n} = n, s, w, e \tag{5.8}$$

The viscosity versus shear rate relationship as predicted by the rheological equations of blood based on the parametric values given in the following table7.

Table 9. Parametric Values for Non-Newtonian Constitute Equations

Parameters	Values
Power law index in Carreau model(n)	0.344
Zero shear rate limit(μ_0)	0.0456Pa.s
Infinite shear rate limit(μ_∞)	0.0032Pa.s
Relaxation time constant(λ)	10.03s
Ideal mean velocity of blood	0.35 m/s

5.3 Summary

In carreau model for pseudo-plastic blood flow, or incompressible Newtonian fluids, the shear stress is proportional to the rate-of-deformation tensor $\overline{\overline{D}}$; For non-Newtonian fluids, the shear stress can similarly be written in terms of a non-Newtonian viscosity $\mu(\dot{\gamma})$.

Figure49 illustrated the velocity distribution of the blood flow in a cross-section and the maximum velocity at the centerline of the artery in the contour is around 0.685 m/s (Figure 49. (a)). Correspondingly, the viscosity in the artery is shown in Figure 49.(b). In the non-Newtonian blood flow, viscosity is not independent of flow at all flow velocities.

As illustrated in the Figure 50, the calculator points to the stable converged pressure gradient value around 1.5 kPa/m to correspond to the mean velocity nearly 35cm/s(0.35m/s) set in the Table 8.

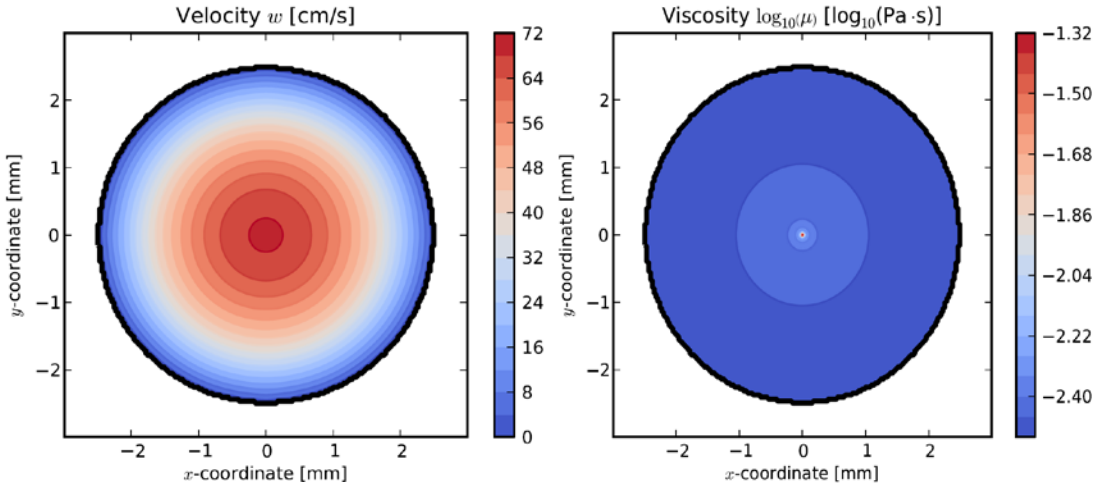

Figure 49: (a). Velocity distribution of the blood flow in a cross-section; (b).Viscosity distribution of the blood flow in a cross-section

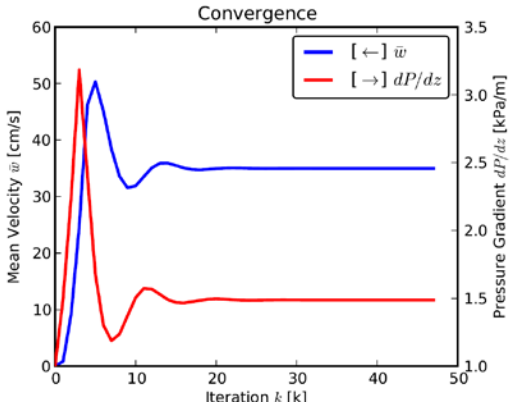

Figure 50: Comparison of the mean velocity and pressure gradient iteration as the iteration tending to a value and program converged

The apparent viscosity of blood decreases as the flow rate is increased. The greater the flow, the greater the rate that one lamina of blood shears against an adjacent lamina. The greater tendency for accumulator in the axial laminae at higher flow rates is partly responsible for this non-Newtonian behavior. However, it is possible that at very slow flow rates, the suspended cells tend to form aggregates, which increases blood viscosity. As flow is increased, this aggregation decreases, and so does the viscosity of blood.

In later research, the computational model employed to quantitatively characterize the hemodynamic conditions under simulated blood flow conditions in a an idealized model of artery. It will progress the potential application of computational blood flow simulations to stent implantation.

REFERENCES

[1] Kochanek KD, Xu JQ, Murphy SL, Minino AM, Kung HC. Deaths: final data for 2009. National vital statistics reports. 201; 60(3).

[2] W. Rosamond, K. Flegal, K. Furie, A. Go, K. Greenlund, N. Haase, S. M. Hailpern, M. Ho, V. Howard, B. Kissela, S. Kittner, D. Lloyd-Jones, M. McDermott, J. Meigs, C. Moy, G. Nichol, C. O'Donnell, V. Roger, P. Sorlie, J. Steinberger, T. Thom, M. Wilson, Y. Hong, American Heart Association Statistics Committee, and Stroke Statistics Subcommittee. Heart Disease and Stroke Statistics – 2008 Update, volume 117. A Report From the American Heart Association Statistics Committee and Stroke Statistics Subcommittee, 2008.

[3] Robbins, S. L, K. Vinay, Robbins and Cotran pathologic basis of disease, 8th edition, Philadelphia, PA, Saunders/Elsevier, 2010.

[4] online link: http://umm.edu/search-results?q=Atherosclerosis

[5] online link: http://www.webmd.com/heart-disease/atherosclerosis-and-coronary-artery-disease

[6] NHLBI report online link: http://www.nhlbi.nih.gov/health/healthtopics/topics/atherosclerosis/treatment last accessed March 2015.

[7] A. Fortier, V. Gullapalli, R.A. Mirshams, Review of Biomechanical Studies of Arteries and Their Effect on Stent Performance, International Journal of Cardiology,Vol.4, 12-18, 2014;

[8] Scot Garg, MB, CHB, Coronary Stents looking forward, Journal of the American College of Cardiology. Vol.56, 2010;10:0735-1097

[9] S. Garg, P.W. Serruys, Coronary Stents: Current Status, Journal of American College of Cardiology 56, 2010; S1-S42

[10] online link: http://en.wikipedia.org/wiki/Drug-eluting_stent.

[11] Subhash Banerjee, MD; Tony S. Das, MD; Mazen S. Abu-Fadel, MD; Eric J. Dippel, MD, Nicolas W. Shammas, MD; Daniel L. Tran, MSc; Ahmad Zankar, MD Cyril Varghese, MS; Kevin C. Kelly, PharmD; Rick A. Weideman, PharmD; Bertis B. Little, PhD; Robert F. Reilly, MD; Tayo Addo, MD; Emmanouil S. Brilakis, MD, PhD, Pilot Trial of Cryoplasty or Conventional Balloon Post-Dilation of Nitinol Stents for Revascularization of Peripheral Arterial Segments-The COBRA Trial, J Am Coll Cardiol. 2012;60(15):1352-1359.

[12] Ormiston JA, Serruys PWS. Bioabsorbable coronary stents. Cir. Cardiovasc Interv 2009;2:255– 60.

[13] online link: http://www.medivisuals.com/an-arterial-wall-604089r-02x.aspx.

[14] Encyclopedia Britannica Inc. 2008.

[15] Klein AJ, Chen SJ, Messenger JC, Hansgen AR, Plomondon ME, Carroll JD, et al. Quantitative assessment of the conformational change in the femoropopliteal artery with leg movement. Catheter Cardiovasc Interv 2009;74:787–98.

[16] T. R. Welch, Advances in Helical Stent Design and Fabrication Thermal Treatment and Structural Interaction Studies of the Simulated Plaque-Laden Artery, Dissertation, Dallas TX, 2009.

[17] D. Stoeckel, C. Bonsignore 1, and S. Duda. Min Invas Ther and Allied Technol 2002: 11(4) 137-147.

[18] Schillinger M, Sabeti S, Dick P, et al. Sustained benefit at 2 years of primary femoropopliteal stenting compared with balloon angioplasty with optional stenting. Circulation. 2007; 115: 2745 – 2749.

[19] Schillinger M, Minar E. Past, present and future of femoropopliteal stenting. J. Endovasc Ther. 2009; 16 Suppl 1 : 147- 152.

[20] Krankenberg H, Schluter M, Steinkamp HJ, et al. Nitinol stent implantation versus percutaneous transluminal angioplasty in superficial femoral artery lesions up to 10cm in length: the femoral artery stenting trial (FAST). Circulation. 2007; 116:285-292.

[21] N. Foin, Drug Eluting Stents Designs and Bifurcation Bench Stenting, Innovations in Cardivascular Intervetions, December 2012, Tel-Aviv Israel.

[22] Roy CS. The elastic properties of the arterial wall. J Physiol 2008 ; 3(125–159):1880–2.

[23] Bergel DH. The visco-elastic properties of the arterial wall. [PhD thesis] University of London; 1960.

[24] Fung YC. On the foundations of biomechanics. J Appl Mech 1983;50:1003–9.

[25] Vaishnav RN, Vossoughi J. Estimation of residual strains in aortic segments. In: Hall CW, editor. Biomedical engineering II: recent developments. New York: Pergamon Press; 1983. 330–333.

[26] online link: http://www.webmd.com/heart-disease/atherosclerosis-and-coronary-artery-disease

[27] Cheng CP, Wilson NM, Hallett RL, et al. In vivo MR angiographic quantification of axial and twisting deformations of the superficial femoral artery resulting from maximum hip and knee flexition. J Vasc Interv Radiol. 2006; 17: 979 – 987.

[28] Smouse HB, Nikanorov A, Laflash D. Biomechanical forces in the femoropopliteal arterial segment. Endovascular Today; June 2005

[29] Stone PH, Coskun AU, Yeghiazarians Y, Kinlay S, Popma JJ, Kuntz RE, Feldman CL. Prediction of sites of coronary atherosclerosis progression: In vivo profiling of endothelial shear stress, lumen, and outer vessel wall characteristics to predict vascular behavior. Curr Opin Cardiol 2003; 18:458-470

[30] Glagov S, Weisnber E, Zarins CK, Stankunavicius R, Kolettis GJ. Compensatory Enlargement of Human Atherosclerotic Coronary Arteries. N Engl J Med. 1987, 316. 1371-1375.

[31] Shiomi M, Yamada S, Matsukawa A, Itabe H, Ito T. Invasion of atheromatous plaques into tunica media causes coronary outward remodeling in WHHLMI rabbits. Atherosclerosis. 2008, 198. 287-293.

[32] Berry JL, Manoach E, Mekkaoui C, Rolland PH, Moore JE Jr, Rachev A. Hemodynamics and Wall Mechanics of a Compliance Matching Stent: In Vitro and In Vivo Analysis. *J Vasc Interv Radiol.* 13, 2002. 97-105.

[33] Feldman CL, Ilegbusi OJ, Hu Z, Nesto R, Waxman S, Stone PH. Determination of in vivo velocity and endothelial shear stress patterns with phasic flow in human coronary arteries: A methodology to predict progression of coronary athersclerosis. Am Heart J 143, 2002. 931-939.

[34] LaDisa JF Jr, Olson LE, Douglas HA, Warltier DC, Kersten JR, Pagel PS. Alterations in regional vascular geometry produced by theoretical stent implantation influence distributions of wall shear stress: analysis of a curved coronary artery using 3D computational fluid dynamics modeling. Biomedical Eng. Online 5:40, 2006.

[35] Lally C., Dolan F., Prendergast P.J. Cardiovascular stent design and vessel stresses: a finite element analysis. J. Biomech. 38, 2005. 1574-1581.

[36] Wu W, Wang WQ, Yang DZ, Qi M. Stent expansion in curved vessel and their interactions: A finite element analysis. J Biomech. 2007. 40. 2580-2585.

[37] Colombo A, Stankovic G, Moses JW. Selection of coronary stents. J Amer Coll Cardiol. 40, 2002. 1021-1033.

[38] Rutsch, W., Kiemeneij, F., Colombo, A., Macaya, C., Guermonprez, J.-L., Grip, L., Hamburger, J., Umans, V., Gotsman, M., Almagor, Y., Morice, M.-C., Garcia, E., Chevalier, B., Erbel, R., Cobaugh, M., Morel, M.-A., Serruys, P.W., 2000. Clinical and angiographic results with the NIR stent:First International NIR Endovascular Stent

[39] Study (FINESS-II). International Journal of Cardiovascular Intervention 3, 143-150. 50. Medtronic DISTANCE trial:whitepaper reporting on the direct stenting with angiographic and clinical evaluation of the S7 (DISTANCE) trial:medtron ic AVE, UC200203607EE 6M 5/02.

[40] Cheng C, Choi; G, Herfkins; R, Taylor CA.The effect of aging on deformations of the superficial femoral artery resulting from hip and knee flexion: potential clinical implications. JVascInterv Radiol 2010;21:195-202.

[41] Ganguly A, Simons J, Schneider A, Keck B, Bennett NR, Herfkins RJ, et al. In-vivo imaging of femoral artery nitinol stents for deformation analysis. JVascInterv Radiol 2011; 22:244-9.

[42] Nikanorov A, Smouse HB, Osman K, Bialas M, Shrivastava S,Schwartz LB. Fracture of self-expanding nitinol stents stressed in-vitro under simulated intravascular conditions. JVascSurg 2008;48:435-40.

[43] Nikanorov A, Schillinger M, Zhao H, Minar E, Schwartz LB. Assessment of self-expanding nitinol stent deformations implanted into the femoropopliteal artery [Abstract]. JVascSurg2009; 49(5Suppl):S24.

[44] Cheng C, Wilson NM, Hallett RL, Herfkens RJ, Taylor CA. In-vivo MR angiographic quantification of axial and twisting deformations of the superficial femoral artery resulting from maximum hip and knee flexion. JVascIntervRadiol 2006; 17:979-87.

[45] Diaz JA, Villegas M, Tamashiro G, Micelli M H, Enterrios D, Balestrini A,et. al. Flexion soft hepopliteal artery: dynamic angiography. JInvasiveCardiol2004; 16:712-5.

[46] Wood NB, Zhao SZ, Zambanin A, Jackson M, Gedroyc W, Thom SA, et al. Curvature and tortuosity of the superficial femoral artery: a possible risk factor for peripheral arterial disease. JAppPhys 2006;101:1412-8.

[47] Wensing PJ, Scholten FG, Buijs PC, Hartkamp MJ, Malk WP, Hillen B. Arterial tortuosity in the femoro popliteal region during knee flexion:amagnetic resonance angiographic study.JAnat1995;186: 133-9.

[48] Brown R, Nguyen TD, Spincemaille P, Prince MR, Wang Y. In-vivo quantification of femoral-popliteal compression during isometric thigh contraction:assessment using MRangiography. JMagnReson Imaging 2009;29:1116-24.

[49] Wensing PJ, Scholten FG, Buijs PC, Hartkamp MJ, Malk WP, Hillen B. Arterial tortuosity in the femoro popliteal region during knee flexion:amagnetic resonance angiographic study.JAnat1995;186: 133-9.

[50] Brown R, Nguyen TD, Spincemaille P, Prince MR, Wang Y. In-vivo quantification of femoral-popliteal compression during isometric thigh contraction:assessment using MRangiography. JMagnReson Imaging 2009;29:1116-24.

[51] Smedby O, Hogman N, Nilsson S, Erikson U, Olsson AG, Walldius G. Two-dimensional tortuosity of the superficial femoral artery in early atherosclerosis. JVascRes1993;30:181-91.

[52] Adams GJ, Baltazar U, Karmonik C, Bordelon C, Lin PH, Bush RL, et al. Comparison of 15 different stents in superficial femoral arteries by high resolution MRI exvivo and invivo. JMagnResonImaging 2005;22:125-35.

[53] Choi G, Cheng CP, Wilson NM, Taylor CA. Methods for quantifying three-dimensional deformation of arteries due to pulsatile and non- pulsatile forces: implications for the design of stents and stent grafts. Ann Biomed Eng2009; 27:14-33.

[54] Ganguly A, Simons J, Schneider A, Keck B, Bennett NR, Herfkens RJ, et al. Invitro imaging of femoral artery Nitinol stents for deformation analysis. J Vasc Interv Radiol 2011;222:244-9.

[55] Klein AJ,Casserly IP, Messnge JC, Carroll JD, ChenS Y. In-vivo3D modeling of the femoro popliteal artery in human subjects based on X-ray angiography: methodology and validation. Med Phys 2009; 362: 289-310.

[56] Müller-Hülsbeck S, Schäfer PJ,Charalambous N,Yagi H, Heller M, JahnkeT.Comparison of second-generation stents for application in the superficial femoral artery:aninvitro evaluation focusing on stent design. J Endovasc Ther 2010; 176:767-76.

[57] Wissgott C,Schmidt W, Behrens P, Schmitz KP, Andresen R. Performance characteristics of modern self-expanding nitinol stents indicated for SFA.RoFo 2009; 181:579-86.

[58] Smouse B, Nikanorov A, LaFlash D.Changes in major peripheral arteries during joint movement before and after stent placement in the cadaver model.

[59] Presented at: Transcatheter Cardiovascular Therapeutics, September 26 - October 4, 2004,Washington,D.C.

[60] Nikanorov A. Arterial biomechanical forces and deformations. Pre-sented at: Stent Summit, Cleveland Clinic, July31 - August2, 2008, Cleveland, Ohio.

[61] Nikanorov A. Multiscale modeling for evaluation of peripheral stent mechanical performance. Presented at: Transcatheter Cardiovascular Therapeutics, September 21-25, 2010, Washington,D.C.

[62] F. Ansari, L.K. Pack, S.S. Brooks, and T. M. Morrison, Design Considerations for studies of the biomechanical environment of the femoropopliteal arteries, Journal of Vascular Surgery, volume 58, Number 3, 2013.

[63] Migliavacca, F., L. Petrini, V. Montanari, I. Quagliana, F. Auricchio, and G. Dubini. A predicative study of the mechanical behavior of coronary stents by computer modeling. Med. Eng. Phys. 27, 2005.13–18.

[64] Topol EJ. Textbook of Interventional Cardiology, 4th Ed; Topol EJ; Saunders: Philadelphia, Pennsylvania, 2003, pp 381-475.

[65] Etave, Mechanical properties of coronary stents determined by using finite element analysis, Journal of Biomechanics, 34, 1065-1075, 2001

[66] Serope Kalpakjian, Steven R. Schmid, Manufacturing Engineering and Technology, 6th Edition, Prentice Hall, 2010.

[67] Edition Authors: Steven R. Schmid, University of Notre Dame; Bernard J. Hamrock, Ohio State University; and Bo. O. Jacobson, Lund University, Sweden, Fundamentals of Machine Elements, 3rd , Prentice Hall, 2004.

[68] online link: http://biomedical.materialise.com/mis

[69] online link: http://www.mscsoftware.com/en-asean/node/970

[70] online link: http://www.healthline.com/health/atherosclerosis

[71] A. Abel, Historical Perspectives and Some of the Main Features of the Bauschinger Effect, Mater. Forum, 1987, 10, 11-26

[72] A. C. Morton, D. Crossman, The influence of physical stent parameters upon restenosis, Journal of Pathology and Biology, 196-205, 2004.

[73] L. Gu, S. Zhao, Arterial Wall Mechanics and Clinical Implications after Coronary Stenting: Comparisons of Three Stent Designs, International Journal of Applied Mechanics, 67-81, 2012.

[74] Linxia Gu, et al, Arterial wall mechanics and clinical implication after coronary stenting: comparisons of three stent desgins, International Journal of Applied Mechanics 4:2,1250013, 2012

[75] H. Henkes, E. Miloslavski, Treatment of intracranial atherosclerotic stenoses with balloon dilatation and self-expanding stent deployment, INTERVENTIONAL NEURORADIOLOGY, 2005, 222-228

[76] Nicholas Karnessis, add all authors, "Uniaxial and buckling mechanical response of auxetic cellular tubes", Smart Materials and Structures, 22 – 31, 2013.

[77] V. Kumar, Robbins and Cotran, Pathologic Basis of Disease, 7th edition, Elsevier Saunders, 2005

[78] P.Ponvin, J. Proft. Stent Tubing: Understanding the Desired Attributes. Medical Device Materials: Proceedings from the Materials & Processes for Medical Devices Conference, DOI: 10.1361, 2004, Pages 253-259

[79] I.G. Masters and K.E. Evans, Models for the elastic deformation of honeycombs, Composite Structure, 1996, 403-422

[80] Zahora, J.,Bezrouk,A.,Hanus,J.,Modeling of stents - comparison and application, Physiol, 2007, 115-121

[81] Graeham R. Douglas, A. Srikantha Phani, Analyses and design of expansion mechanisms of balloon expandable vascular stents, Journal of biomechanics, Issue6, 2014, 1438-1446

[82] Nasim Paryab, Duane S Cronin, Finite element methods to analyze helical stent expansion, International Journal for numerical methods in biomedical Engineering, 2014, 339-352

[83] Alessio Meoli, Elena Dordoni,et al, Computational Study of Axial Fatigue for Peripheral nitinol stents,Journal of Materials Engineering and Performance, 2014, 2606-2613

[84] Garasic, Joseph M., Stent and Artery Geometry Determine Intimal Thickening Independent of Arterial Injury,Journal of the American Heart Association,2000,812-818

[85] F Auricchio, A Constantinescu, Fatigue of 316L stainless steel notched [mu] m-size components, International Journal of Fatigue, 2014-11-01, 231

[86] Online: Free pipe stress analysis
http://www.efunda.com/formulae/solid_mechanics/mat_mechanics/pressure_vessel.cfm

[87] Dimitrios E. Kiousis, et.al. Experimental Studies and Numerical Analysis of the Inflation and Interaction of Vascular Balloon Catheter-Stent Systems, Anals of Biomedical Engineering. 2009, 315-330

[88] Lucas H. Timmins, Michael R. Moreno, Stented artery biomechanics and device design optimization,Med Bio Eng Comput, 2007, 505-513

[89] Lucas H Timmins, Matthew W Miller et. al, Increased artery wall stress post-stenting leads to greater intimal thickening, Laboratory Investigation, 2011, 91, 955-967

[90] Updated Lagrangian formulation for incremental general nonlinear analysis. MIT online course. Topic 5. http://ocw.mit.edu/resources/res-2-002-finite-element-procedures-for-solids-and-structures-spring-2010/nonlinear/lecture-5/MITRES2_002S10_lec05.pdf

[91] Online: http://www.480biomedical.com/products/stanza-bioresorbable-scaffold

[92] Ruipeng Li, Yunfeng Zhang, et al, Numerical study of the cyclic load behavior of AISI 316L stainless steel shear links for seismic fuse device, Front. Struct. Civ. Eng., 2014,vol.8 414-426

[93] Glagov S, Zarins C, Giddens DP, Ku DN., Hemodynamics and atherosclerosis:insights and perspectives gained from studies of human arteries, Arch. Pathol. Lab. Med., 1988, 1018-1031

[94] Julian Bedoya, Clark A. Meyer, Effects of Stent Design Parameters on Normal Artery Wall Mechanics, Journal of Biomechanical Engineering, 2006, 757-765

[95] Luke Mizzi, Daphne Attard, On the suitability of hexagonal honeycombs as stent geometries, Phys. Status Solidi B, 2014, 328-337

[96] Haldar, K., Effects of the shape of stenosis on the resistance of blood flow through an artery, Bulletin of Mathematical Boilogy,1985, 545-550

[97] Mir Golam Rabby, Sumaia Parveen Shupti, and Md. MamunMolla, Pulsatile Non-Newtonian Laminar Blood Flows through Arterial Double Stenoses, Journal of Fluids, 2014, 1-13